Advances in Nano Research, *Vol. 14, No. 5 (2023) 475-493*
https://doi.org/10.12989/anr.2023.14.5.475

Dynamic vibration response of functionally graded porous nanoplates in thermal and magnetic fields under moving load

Ismail Esen[1], Mashhour A. Alazwari[2], Khalid H. Almitani[2], Mohamed A Eltaher*[2,3] and A. Abdelrahman[3]

[1]*Department of Mechanical Engineering, Karabuk University, Karabuk, Turkey*
[2]*Mechanical Engineering Department, Faculty of Engineering, King Abdulaziz University, P.O. Box 80204, Jeddah, Saudi Arabia*
[3]*Mechanical Design & Production Department, Faculty of Engineering, Zagazig University, P.O. Box 44519, Zagazig, Egypt*

(*Received February 6, 2022, Revised September 26, 2022, Accepted October 4, 2022*)

Abstract. In the context of nonclassical nonlocal strain gradient elasticity, this article studies the free and forced responses of functionally graded material (FGM) porous nanoplates exposed to thermal and magnetic fields under a moving load. The developed mathematical model includes shear deformation, size-scale, miscorstructure influences in the framework of higher order shear deformation theory (HSDT) and nonlocal strain gradient theory (NSGT), respectively. To explore the porosity effect, the study considers four different porosity models across the thickness: uniform, symmetrical, asymmetric bottom, and asymmetric top distributions. The system of quations of motion of the FGM porous nanoplate, including the effects of thermal load, Lorentz force, due to the magnetic field and moving load, are derived using the Hamilton's principle, and then solved analytically by employing the Navier method. For the free and forced responses of the nanoplate, the effects of nonlocal elasticity, strain gradient elasticity, temperature rise, magnetic field intensity, porosity volume fraction, and porosity distribution are analyzed. It is found that the forced vibrations of FGM porous nanoplates under thermal and live loads can be damped by applying a directed magnetic field.

Keywords: FGM porous nanoplate; magnetic field; moving load; multiphysic domain; nonlocal strain gradient theory; thermal load

1. Introduction

Currently, there is considerable research interest in the size dependent dynamic behavior of small-scale functionally graded porous systems under complex thermal, magnetic and mechanical live loads. These systems are vastly employed as components in various applications such as micro and nano-electro-mechanical systems (MEMS and NEMS), Yaylı (2015, 2016) and Jalaei and Thai (2019). In the framework of nonclassical continuum mechanics, this study investigates the nonclassical free and forced vibration response of a functionally graded porous nanoplate in thermomagnetic environment and exposed to a moving load based on the higher shear deformation (HSDT) and the nonlocal strain gradient theory (NSGT).The nanoplate consists of ceramic and metal constituents that are graded through the plate thickness according to the power-law, and porosity is inevitable due to the nature of such structures. In addition, in specific areas of use, it may be desirable to create porosity for lightweight structures by design.

In nanoscale systems, the classical theories are insufficient for predicting actual stresses. For this reason, the micro-morphic theory (MMT), defined by (Eringen and Suhubi 1964), the nonlocal elasticity theory (NET) (Eringen 1983), the strain gradient elasticity theory (SGET) (Kong *et al*. 2008), the modified couple stress theory (MCST) (Ke *et al.* 2012, Kong *et al.* 2008), the surface elasticity theory (SET) (Ansari *et al.* 2015), and the nonlocal strain gradient theory (NSGT) (Li and Hu, 2015) have been proposed to efficiently incorporate the nonclassical phenomena in the nanoscale systems such as the nonlocality effect, strain gradient effect, the microstructure effect, surface elasticity effect, and the combined nonlocal strain gradient effect.

Recently, porous small-scale structures subjected to various loading conditions are earned great importance due to several applicability of these systems in micro and nano-electro-mechanical systems (MEMS and NEMS). Applying the NET, both static and free vibration behaviors of FGM porous nanobeams have been studied by Eltaher *et al.* (2016, 2018, 2019) using the Euler Bernoulli beam theory (EBBT) and NET. Yayli (2018a, b, c, 2020) predicted the longitudinal. transverse, and rotational frequencies of microbars and microbeams using NET. Yayli (2019a, b) enhanced previous works to included the effect of rotational restraints on the free vibration analysis. The nonlinear buckling of FGM porous beams has been investigated by Shafiei and Kazemi (2017) using the EBBT and NET. The effect of porosity is also a major research topic in large-scale structures. Several studies had been performed to study the static and dynamic behavior of porous structures such as regular conventional beams, curved beams, sandwich beams using various shear theories with analytical and finite element methods. (Askari *et al.* 2021, Azartash *et al.* 2021, Chen *et al.* 2020, 2016, Chinh *et al.* 2021, Dang and Do, 2021, Derikvand *et al.* 2021, Ebrahimi *et al.* 2016, Ebrahimi and Jafari, 2016, Eltaher *et al.* 2018, Faroughi *et al.* 2020, Jankowski *et al.* 2021, Merzouki *et al.* 2021,

*Corresponding author, Professor, Ph.D.,
E-mail: meltaher@kau.edu.sa; mmeltaher@zu.edu.eg

ISSN: 2287-237X (Print), 2287-2388 (Online)

Nikrad *et al.* 2021, Rahmani *et al.* 2020a, b, Salari *et al.* 2020, She *et al.* 2019, Wang *et al.* 2018, Wu *et al.* 2018, Xu *et al.* 2021).

Several studies have been developed to study the multi-physics problems of nanostructures in thermomagnetic environments. Based on the Timoshenko beam theory (TBT), Jalaei and Civalek (2019) have investigated the nonclassical dynamic instability of a FGM porous nanobeam resting on a viscoelastic foundation and subjected to a magnetic field using the NET. To explore the influence of porosity distribution across the beam thickness, Ghandourah and Abdraboh (2020) and Ghandourah (2021) have studied the size dependent dynamic behavior of FGM porous nanobeam with different porosity models based on the EBBT and NET. Based on the higher-order shear deformation theory (HSDT) and the general nonlocal theory (GNT), the wave propagation in rotating two dimensional (2D) FGM porous nanobeam has been studied by Faroughi *et al*. (2020). To investigate the viscosity effect on the nonclassical dynamic behavior of nanobeams, Liu *et al.* (2018) studied the vibration of FGM magneto-electro-viscoelastic porous nanobeams based on the TBT and NET. Introducing the hygro-thermal effect, Penna *et al.* (2021a, b) studied the nonclassical hygro-thermal bending and vibration responses of FGM porous nanobeam using the EBBT, the NET and the NSGT.

The need to new materials with the improved properties is the objective of engineers and scientists. Even though, traditional laminated composite materials are being extensively used in the aircrafts, space crafts, shipbuilding, automotive and various other industries, they have some limitations that can be improved by using FGMs, (Gayen *et al*. 2019 and Li *et al*. 2020). Properties of the FGMs can be altered reliant to various biomedical applications, such as teeth and human bone, Boggarapu *et al*. (2021). In addition, FGM can be used in manufacture of Rotor-Bearing System and shafts, Gayen *et al*. (2021) and Gayen (2022). FGMs can be manufactured by different techniques such as centrifugal force methods, powder metallurgy methods, vapour deposition methods and the additive manufacturing methods, Saleh *et al*. (2020). Various studies have been performed to investigate the mechanical size dependent of the functionally graded porous nano-size plates. The effect of the porosity is a new research issue and recent. The free vibration response of FGM porous macro/micro/nanoshell and plates has been given by Bendaho *et al*. (2019) and Talebizadehsardari *et al*. (2020) using the HSDT and the NSGT. The free vibration behavior of FGM porous nanoplates resting on a two-parameter foundation has been given by Doan *et al*. (2021) using the first order share deformation theory (FSDT) and the NET. Esmaeilzadeh *et al*. (2021) studied geometrically nonlinear thermo-mechanical analysis of graphene-reinforced moving polymer nanoplates.

As illustrated in the above literature, the studies on FGM porous nanoplates are limited in the literature and have only addressed the free response of porous nanoplates with uniform and random porosity distributions. For this reason, this work deals with the nonclassical free and forced responses of porous nanoplates in the thermal and magnetic environments under moving load. The proposed model

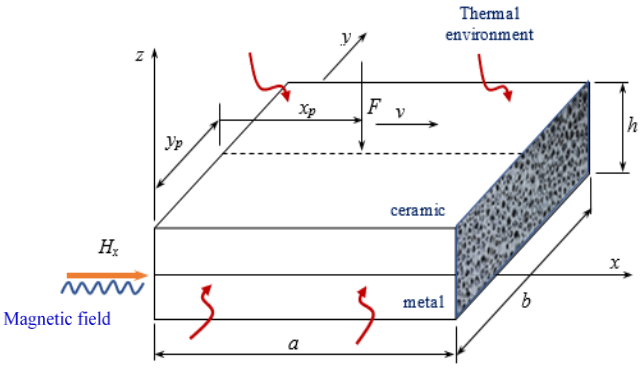

Fig. 1 Configuration of a thick FGM porous nanoplate in thermal and magnetic fields

considers four different porosity distributions models of FGM nanoplates using the HSDT and NSGT. Based on the Navier analytical methodology, the system of equations of motion is solved for both free and forced vibration analyses. Moreover, effects of porosity distribution, non-local, size dependent parameters, thermal and Lorentz forces, and interaction with live load are analyzed and some interesting new results are presented such as the free and forced vibrational stability of FGM porous nanoplates under severe conditions can be improved using the intensity of a directed magnetic field.

2. Effective properties of FGM porous nanoplates

Fig. 1 shows a porous FGM nanoscale plate in a thermal environment subjected to a horizontal x-direction magnetic field and a moving point load.

2.1 Temperature-dependent material properties

Metal and ceramic material constituents are temperature-dependent and effective material properties can be defined as (Touloukian, 1967):

$$P = P_0(P_{-1}T^{-1} + 1 + P_1T + P_2T^2 + P_3T^3) \quad (1)$$

As given in Table.1, the symbols P_0, P_{-1}, P_1, P_2, and P_3 are experimentally defined specific material values based on degrees of temperature T. Because of the nano-size, a uniform temperature rise case is only managed with a stress-free state at (T_0 = 300 K), where $\Delta T = T - T_0$.

2.2 Porosity models and effective properties

The effective material properties in the plate can be defined by the volume fractions V_c and V_m and properties P_c and P_m of ceramic and metal constituents, considering a power-law grading with the following formula. (Najafi *et al.* 2017, Ebrahimi *et al*. 2021)

$$\begin{aligned} P_{ef} &= V_cP_c + V_mP_m \\ V_c &= \left(\frac{z}{h} + \frac{1}{2}\right)^n, V_m = 1 - V_c \\ V_c 0 &\le n < \infty \end{aligned} \quad (2)$$

where V_c, V_m, and n are respectively the ceramic volume

Table 1 Temperature dependent coefficients of the properties (Reddy and Chin 1998)

Material	Property	P_{-1}	P_0	P_1	P_2	P_3
	E (Pa)		348.43x10^9	-3.070x10^{-4}	2.160x10-7	-8.946x10^{-11}
	υ		0.24	0	0	0
Si_3N_4	α (1K^{-1})	0	5.8723x10^{-6}	9.095x10^{-4}	0	0
	ρ (kg/m^3)		2370	0	0	0
	ψ (W/mK)		13.729	-1.032x10^{-3}	5.466 X 10 $^{-7}$	-7.876 x10^{-11}
	E (Pa)		201.04x 10^9	3.079x10^{-4}	-6.534x10^{-7}	0
	υ		0.3262	-2.002x10^{-4}	3.97x10-7	0
SUS304	α (1K^{-1})	0	12.33x10^{-6}	8.086x10^{-4}	0	0
	ρ (kg/m^3)		8166	0	0	0
	ψ (W/mK)		15.397	-1.264x10^{-3}	2.092x10^{-6}	-7.223x10^{-10}

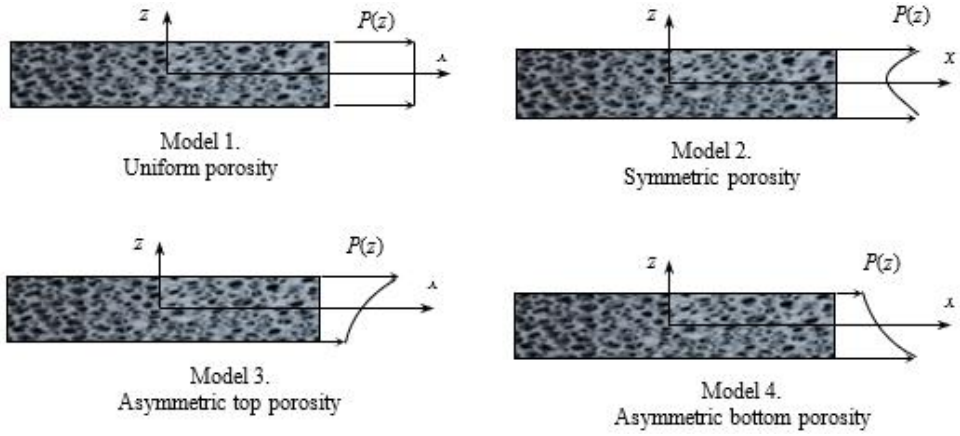

Fig. 2 Four models of porosity distribution across the plate thickness

fraction, the metal volume fraction, and the material grading index. According to Eq. (2), any material property, P(z) such as the material density, the modulus of elasticity, the Poisson ratio, and the thermal expansion coefficient of FGM plate with no porosity are obtained as follows. (Reddy and Chin, 1998):

$$P(z) = [P_c - P_m]V_c + P_m \tag{3}$$

In this study, four types of porosity distributions across the thickness are considered as given in Fig. 2. Accordingly, the effective material properties are obtained by substituting the total volume fraction (α) of porosity in Eq. (2). Thus, by using Eq. (2), the following porosity distribution models are respectively given as follows, Ebrahimi *et al.* (2021), Najafi *et al.* (2017):

$$P(z) = \begin{cases} [P_c - P_m]V_c + P_m - \dfrac{\alpha}{2}[P_c + P_m] \\ \text{Uniform (model 1)} \\ \{[P_c - P_m]V_c + P_m\}\left\{1 - \alpha\cos\left[\pi\dfrac{z}{h}\right]\right\} \\ \text{Symmetric (model 2)} \\ \{[P_c - P_m]V_c + P_m\}\left\{1 - \alpha\cos\left[\dfrac{\pi}{2}\left(\dfrac{z}{h} + \dfrac{1}{2}\right)\right]\right\} \\ \text{Asymmetric top (model 3)} \\ \{[P_c - P_m]V_c + P_m\}\left\{1 - \alpha\cos\left[\dfrac{\pi}{2}\left(\dfrac{z}{h} - \dfrac{1}{2}\right)\right]\right\} \\ \text{Asymmetric bottom (model 4)} \end{cases} \tag{4}$$

Based on the NGST, for a small-scale plate, the stress strain constitutive relations are derived as (Jalaei and Thai 2019, Lim *et al.* 2015):

$$\left[1 - (ea)^2\nabla^2\right]\begin{Bmatrix}\sigma_{xx}\\ \sigma_{yy}\\ \tau_{xy}\\ \tau_{yz}\\ \tau_{xz}\end{Bmatrix} = \left[1 - l_m^2\nabla^2\right]Q_{ij}\begin{Bmatrix}\varepsilon_{xx}\\ \varepsilon_{yy}\\ \gamma_{xy}\\ \gamma_{yz}\\ \gamma_{xz}\end{Bmatrix}, \tag{5}$$

$Q_{ij}, (ij = 11, 12, 22, 44, 55, 66),$

where σ_{ij}, τ_{ij} and $\varepsilon_{ij}, \gamma_{ij}$ are respectively the normal and shear stress and strains, and the stiffnesses Q_{ij} are:

$$Q_{11} = Q_{22} = \frac{E(z)}{1-\upsilon^2}, \quad Q_{12} = \frac{\upsilon E(z)}{1-\upsilon^2}, \\ Q_{44} = Q_{55} = Q_{66} = \frac{E(z)}{2(1+\upsilon)}. \tag{6}$$

3. Adapting NSGT to thick nanoplate

3.1 Constitutive Relations

Based on the HSDT, the displacement field is in the form (Aghababaei and Reddy 2009, Akavci 2014)

$$\begin{Bmatrix} u(x,y,z,t) \\ v(x,y,z,t) \\ w(x,y,z,t) \end{Bmatrix} = \begin{bmatrix} 1 & 0 & -z\frac{\partial}{\partial x} & f(z) & 0 \\ 0 & 1 & -z\frac{\partial}{\partial y} & 0 & f(z) \\ 0 & 0 & 1 & 0 & 0 \end{bmatrix} \begin{Bmatrix} u_0(x,y,t) \\ v_0(x,y,t) \\ w_0(x,y,t) \\ \phi_x(x,y,t) \\ \phi_y(x,y,t) \end{Bmatrix}, \quad (7)$$
$$f(z) = z\left(1 - \frac{4}{3}\left(\frac{z}{h}\right)^2\right),$$

here, $u(x,y,z,t)$, $v(x,y,z,t)$, and $w(x,y,z,t)$ are the displacements and $u_0(x,y,t)$, $v_0(x,y,t)$ and $w_0(x,y,t)$ represent the mid-plane displacements, and $\phi_x(x,y,t)$ and $\phi_y(x,y,t)$ are the rotation of the cross-section, and $(.)_{,x}$ and $(.)_{,y}$ are partial derivatives for x and y, and $f(z)$ refers to the shape function. The kinematic strain displacement relations are given as, (Aghababaei and Reddy 2009, Reddy 1984):

$$\begin{Bmatrix} \varepsilon_{xx} \\ \varepsilon_{yy} \\ \gamma_{xy} \\ \gamma_{yz} \\ \gamma_{xz} \end{Bmatrix} = \begin{Bmatrix} \frac{\partial u_0(x,y,t)}{\partial x} - z\frac{\partial^2 w_0(x,y,t)}{\partial x^2} + f(z)\frac{\partial \phi_x(x,y,t)}{\partial x} \\ \frac{\partial v_0(x,y,t)}{\partial y} - z\frac{\partial^2 w_0(x,y,t)}{\partial y^2} + f(z)\frac{\partial \phi_y(x,y,t)}{\partial y} \\ \frac{\partial u_0(x,y,t)}{\partial y} + \frac{\partial v_0(x,y,t)}{\partial x} - 2z\frac{\partial^2 w_0(x,y,t)}{\partial x \partial y} \\ +f(z)\left(\frac{\partial \phi_x(x,y,t)}{\partial y} + \frac{\partial \phi_y(x,y,t)}{\partial x}\right) \\ \left(\frac{df(z)}{dz}\right)\phi_y(x,y,t) \\ \left(\frac{df(z)}{dz}\right)\phi_y(x,y,t) \end{Bmatrix} \quad (8)$$

Including the thermal effect, the constitutive relationships of the HSDT and NSGT for the porous FGM nanoplate can be stated as follows:

$$\begin{Bmatrix} \sigma_{xx} \\ \sigma_{yy} \\ \tau_{xy} \\ \tau_{yz} \\ \tau_{xz} \end{Bmatrix} \left[1 - (ea)^2 \nabla^2\right] = \begin{bmatrix} Q_{11} & Q_{12} & 0 & 0 & 0 \\ Q_{12} & Q_{22} & 0 & 0 & 0 \\ 0 & 0 & Q_{66} & 0 & 0 \\ 0 & 0 & 0 & Q_{44} & 0 \\ 0 & 0 & 0 & 0 & Q_{55} \end{bmatrix} \begin{Bmatrix} \varepsilon_{xx} - \alpha_{xx}\Delta T \\ \varepsilon_{yy} - \alpha_{yy}\Delta T \\ \gamma_{xy} \\ \gamma_{yz} \\ \gamma_{xz} \end{Bmatrix} \left[1 - l_m^2 \nabla^2\right]. \quad (9)$$

The stiffnesses, Q_{ij} are as given in (6). And the force and moment resultants can be written as

$$\begin{Bmatrix} N \\ M \\ P \end{Bmatrix} = \begin{bmatrix} A_{ij} & B_{ij} & C_{ij} \\ B_{ij} & D_{ij} & E_{ij} \\ C_{ij} & E_{ij} & G_{ij} \end{bmatrix} \begin{Bmatrix} \varepsilon \\ \kappa \\ \kappa_\phi \end{Bmatrix}, (i,j = 1,2,6), \quad (10)$$

$$\{R\} = [F_{ij}]\{\phi\}, (i,j = 4,5). \quad (11a)$$

where

$$N = \begin{Bmatrix} N_x \\ N_y \\ N_{xy} \end{Bmatrix}, M = \begin{Bmatrix} M_x \\ M_y \\ M_{xy} \end{Bmatrix}, P = \begin{Bmatrix} P_x \\ P_y \\ P_{xy} \end{Bmatrix}, R = \begin{Bmatrix} R_x \\ R_y \end{Bmatrix}, \quad (11b)$$

$$\varepsilon = \begin{Bmatrix} \frac{\partial u_0(x,y,t)}{\partial x} \\ \frac{\partial v_0(x,y,t)}{\partial y} \\ \frac{\partial u_0(x,y,t)}{\partial y} + \frac{\partial v_0(x,y,t)}{\partial x} \end{Bmatrix}, \kappa = \begin{Bmatrix} \frac{\partial^2 w_0(x,y,t)}{\partial x^2} \\ \frac{\partial^2 w_0(x,y,t)}{\partial y^2} \\ 2\frac{\partial^2 w_0(x,y,t)}{\partial x \partial y} \end{Bmatrix}, \quad (11c)$$

$$\kappa_\phi = \begin{Bmatrix} \frac{\partial \phi_x(x,y,t)}{\partial x} \\ \frac{\partial \phi_y(x,y,t)}{\partial y} \\ \frac{\partial \phi_x(x,y,t)}{\partial y} + \frac{\partial \phi_y(x,y,t)}{\partial x} \end{Bmatrix}, \quad \phi = \begin{Bmatrix} \phi_x \\ \phi_y \end{Bmatrix}. \quad (11d)$$

and the stiffness coefficients are described by:

$$\begin{Bmatrix} (A_{ij}, B_{ij}, C_{ij}, D_{ij}, E_{ij}, G_{ij}) \\ F_{ij} \end{Bmatrix} = \begin{Bmatrix} \int_{-\frac{h}{2}}^{\frac{h}{2}} (1, z, f(z), z^2, zf(z), f(z)^2) Q_{ij} dz, \ i,j = 1,2,6) \\ \int_{-h/2}^{h/2} \left(\frac{df(z)}{dz}\right)^2 Q_{ij}\, dz \quad i,j = 4,5 \end{Bmatrix} \quad (12)$$

3.2 Nonclassical dynamic equations of motion of thick nanoplate

Applying the Hamilton principle, Reddy (2007)

$$\int_{t1}^{t2} (\delta T - \delta U + \delta(V_{qT} + V_m) dt = 0 \quad (13)$$

with U refers to the strain energy which can be expressed as

$$U = \frac{1}{2}\int_V (\sigma_{xx}\varepsilon_{xx} + \sigma_{yy}\varepsilon_{yy} + \tau_{xy}\gamma_{xy} + \tau_{xz}\gamma_{xz} + \tau_{yz}\gamma_{yz}) dV \quad (14)$$

while T is the kinetic energy which is given by

$$T = \frac{1}{2}\int_0^a \int_0^b \int_{-h/2}^{h/2} \rho(z)[(\dot{u}^2 + \dot{v}^2 + \dot{w}^2)]\, dz dy dx \quad (15)$$

and V_{qT} is the external potential energy of transverse $q(x,y,t)$ and thermal loads

$$V_{qT} = \int_\Omega \left[q(x,y,t)w_0 - N_{xx}^T \frac{\partial^2 w_0}{\partial x^2} - N_{yy}^T \frac{\partial^2 w_0}{\partial y^2}\right] d\Omega \quad (16)$$

In this study, the nanoscale plate is exposed to the magnetic field and the effect of this field can be obtained by Maxwell's equations (Arani and Jalaei 2017, Kraus 1992). Thus, based on Maxwell's equations, magnetic field vector (h) current density vector (J), magnetic field permeability (η), electric field vector (e), and magnetic field density (H) are described as

$$\mathbf{J} = \nabla \times \mathbf{h}, \quad \nabla \times \mathbf{e} = -\eta \frac{\partial \mathbf{h}}{\partial t}, \quad \nabla \cdot \mathbf{h} = 0. \quad (17)$$

$$\mathbf{e} = -\eta\left(\frac{\partial \mathbf{U}}{\partial t} \times \mathbf{H}\right), \quad \mathbf{h} = \nabla \times (\mathbf{U} \times \mathbf{H}). \quad (18)$$

Here, $\mathbf{U} = u\vec{\imath} + v\vec{\jmath} + w\vec{\mathrm{k}}$, describes the displacement field vector. Assuming the longitudinal magnetic field applied to the microbeam is a vector, where $\mathbf{H} = H_x\vec{\imath}$, the following equation can be written as, Alazwari *et al*. (2022):

$$\mathbf{h} = -H_x\left(\frac{\partial v}{\partial y} + \frac{\partial w}{\partial z}\right)\vec{\imath} + H_x\frac{\partial v}{\partial x}\vec{\jmath} + H_x\frac{\partial w}{\partial x}\vec{\mathrm{k}} \quad (19)$$

The Lorentz force due to the magnetic field is obtained as:

$$f_m = f_{mx}\vec{\imath} + f_{my}\vec{\jmath} + f_{mz}\vec{k} = \eta(\mathrm{J}\times \mathbf{H}) = \eta\begin{bmatrix} 0\vec{\imath} + H_x^2\left(\frac{\partial^2 v}{\partial x^2}+\frac{\partial^2 v}{\partial y^2}+\frac{\partial^2 w}{\partial y\partial z}\right)\vec{\jmath} \\ +H_x^2\left(\frac{\partial^2 w}{\partial x^2}+\frac{\partial^2 w}{\partial z^2}+\frac{\partial^2 v}{\partial y\partial z}\right)\vec{k} \end{bmatrix} \quad (20)$$

If f_m applies in the transverse z-direction only thus, Eq. (20) can be simplified as

$$f_{mz} = \eta H_x^2\left(\frac{\partial^2 w}{\partial x^2}+\frac{\partial^2 w}{\partial z^2}+\frac{\partial^2 v}{\partial y\partial z}\right) \quad (21)$$

Finally, using Eqs. (7) and (21), the Lorentz force is achieved as follows:

$$F_l = \int_{-h/2}^{h/2} f_{mz}dz = \eta h H_x^2\left(\frac{\partial^2 w_0}{\partial x^2} - \frac{\partial^2 w_0}{\partial y^2} + \frac{\partial \phi_y}{\partial y}\right) \quad (22)$$

The virtual work done by external forces and the Lorentz force, V_m is

$$V_m = \int_\Omega (F_l)\, w(x,y,t)d\Omega \quad (23)$$

By substituting Eqs. (14), (15) and (16) into Eq. (13) and after the integration, setting each coefficient of δu_0, δv_0, $\delta w_0, \delta\phi_x$ and $\delta\phi_y$ to zero, the equations of motion are:

$$\left(1 - l_m^2\frac{\partial^2}{\partial x^2}\right)\begin{bmatrix} N_{x,x}+N_{xy,y} \\ N_{xy,x}+N_{y,y} \\ M_{x,xx}+M_{y,yy}+2M_{xy,xy} \\ P_{x,x}+P_{xy,y}-R_x \\ P_{xy,x}+P_{y,y}-R_y \end{bmatrix} = \left(1-(ea)^2\frac{\partial^2}{\partial x^2}\right)\begin{bmatrix} I_1\ddot{u}_0 - I_2\ddot{w}_{0,x} + I_4\ddot{\phi}_x \\ I_1\ddot{v}_0 - I_2\ddot{w}_{0,y} + I_4\ddot{\phi}_y \\ S+\Psi \\ I_4\ddot{u}_0 - I_5\ddot{w}_{0,x} + I_6\ddot{\phi}_x \\ I_4\ddot{v}_0 - I_5\ddot{w}_{0,y} + I_6\ddot{\phi}_y \end{bmatrix} \quad (24)$$

with,

$$\begin{Bmatrix} S \\ \Psi \end{Bmatrix} = \begin{Bmatrix} I_1\ddot{w}_0 + I_2(\ddot{u}_{0,x}+\ddot{v}_{0,y}) - I_3(\ddot{w}_{0,xx}+\ddot{w}_{0,yy}) \\ -I_5(\dot{\phi}_{x,x}+\dot{\phi}_{y,y}) \\ -q - \eta h H_x^2\left(w_{0,xx}-w_{0,yy}+\left[\frac{1}{h}\int_{-\frac{h}{2}}^{\frac{h}{2}}(f(\acute{z}))dz\right]\phi_{y,y}\right) \\ +N_{xx}^T w_{0,xx} + N_{yy}^T w_{0,yy} \end{Bmatrix} \quad (25)$$

and the inertia coefficients:

$$(I_1, I_1, I_2, I_3, I_4, I_5, I_6) = \int_{-h/2}^{h/2}\rho(z)(1, z, z^2 f(z), zf(z), [f(z)]^2)dz \quad (26)$$

The boundary conditions are described using edge displacements and forces as:

$$\begin{pmatrix} \text{at } x \text{ edges:} \\ either\ u\ or\ N_x \\ either\ v\ or\ N_{xy} \\ either\ w\ or\ M_{x,x}+2M_{xy,x} \\ either\ w_{,x}\ or\ M_x \\ either\ \phi_x\ or\ P_x \\ either\ \phi_y\ or\ P_{xy} \end{pmatrix}, \begin{pmatrix} \text{at } y \text{ edges:} \\ either\ v\ or\ N_{xy} \\ either\ u\ or\ N_{xy} \\ either\ w\ or\ M_{y,y}+2M_{xy,x} \\ either\ w_{,y}\ or\ M_y \\ either\ \phi_x\ or\ P_{xy} \\ either\ \phi_y\ or\ P_y \end{pmatrix} \quad (27)$$

3.3 Navier solution for simply supported rectangular nanoplates in thermomagnetic environments

To obtain closed form solution for free and forced vibration behavior of functionally graded porous nanoplate in thermomagnetic environments under live load, the Navier analytical methodology as a simple and efficient procedure is adopted. The classical and nonclassical boundary conditions at the edges of the simply supported nanoplate can be satisfied by:

$$\begin{aligned} at\ x = 0, a: &\quad N_x = v = w = M_x = P_x = \phi_y = 0, \\ at\ y = 0, b: &\quad N_y = u = w = M_y = P_y = \phi_x = 0. \end{aligned} \quad (28)$$

However, non-classical boundary conditions controlled by:

$$\begin{aligned} at\ x = 0, a: &\quad \frac{\partial}{\partial x}\left(N_x, v, w, M_x, P_x, \phi_y\right) = 0 \\ at\ y = 0, b: &\quad \frac{\partial}{\partial y}\left(N_y, u, w, M_y, P_y, \phi_x\right) = 0 \end{aligned} \quad (29)$$

3.3.1 Solution of eigen value problem of nanoplate in thermomagnetic environments

Neglecting the effect of the applied external force vector in Eq. (24), free vibration problem is obtained. To derive closed forms for the resonant frequencies for the considered boundary conditions, the following Fourier series are used for the displacements which satisfy the essential boundary conditions as:

$$\begin{aligned} u_0(x,t) &= \sum_m\sum_n U_{mn}\cos(\alpha x)\sin(\beta y)\, e^{i\omega_{mn}t}, \\ v_0(x,t) &= \sum_m\sum_n V_{mn}\sin(\alpha x)\cos(\beta y)\, e^{i\omega_{mn}t}, \\ w_0(x,t) &= \sum_m\sum_n W_{mn}\sin(\alpha x)\sin(\beta y)\, e^{i\omega_{mn}t}, \\ \phi_x(x,t) &= \sum_m\sum_n \mathrm{X}_{mn}\cos(\alpha x)\sin(\beta y)\, e^{i\omega_{mn}t}, \\ \phi_y(x,t) &= \sum_m\sum_n \mathrm{Y}_{mn}\sin(\alpha x)\cos(\beta y)\, e^{i\omega_{mn}t}. \end{aligned} \quad (30)$$

where $\alpha = \left(\frac{m\pi}{a}\right), \beta = \left(\frac{n\pi}{b}\right)$, $i = \sqrt{-1}$, and ω_{mn} is the natural vibration frequency of the mode (m, n). U_{mn}, V_{mn} W_{mn}, X_{mn} and Y_{mn} are arbitrary coefficients. Substituting Eq. (30) into Eq. (24) the following nonclassical elasto-thermomagnetic eigen value problem is achieved.

$$(\mathbf{K} - \omega_{mn}^2 \mathbf{M})\mathbf{d} = 0. \tag{31}$$

Here, $\mathbf{d} = \{U_{mn} \quad V_{mn} \quad W_{mn} \quad X_{mn} \quad Y_{mn}\}^T$ are the vector of the unknown coefficients, K, and M are stiffness and mass matrices with the following coefficients:

$$\begin{aligned}
\mathrm{K}_{11} &= (A_{11}\alpha^2 + A_{66}\beta^2)c_2 \\
\mathrm{K}_{12} = \mathrm{K}_{21} &= (A_{12} + A_{66})\beta\alpha c_2 \\
\mathrm{K}_{13} = \mathrm{K}_{31} &= -B_{11}\alpha^3 c_2 \\
\mathrm{K}_{14} = \mathrm{K}_{41} &= (C_{11}\alpha^2 + C_{66}\beta^2)c_2 \\
\mathrm{K}_{15} = \mathrm{K}_{24} = \mathrm{K}_{42} = \mathrm{K}_{51} &= (C_{12} + C_{66})\beta\alpha c_2 \\
\mathrm{K}_{22} &= (A_{66}\alpha^2 + A_{22}\beta^2)c_2 \\
\mathrm{K}_{23} = \mathrm{K}_{32} &= -B_{22}\alpha^3 c_2 \\
\mathrm{K}_{25} = \mathrm{K}_{52} &= (C_{66}\alpha^2 + C_{22}\beta^2)c_2 \\
\mathrm{K}_{33} &= (D_{11}\alpha^4 + 2D_{12}\alpha^2\beta^2 + 4D_{66}\alpha^2\beta^2 + D_{22}\beta^4)c_2 \\
&\quad + \left(-N_{xx}^T\alpha^2 - N_{yy}^T\beta^2 \right. \\
&\quad \left. + \eta h H_x^2(\alpha^2 - \beta^2)\right)c_1 \\
\mathrm{K}_{34} = \mathrm{K}_{43} &= -(E_{11}\alpha^3 + (E_{12} + 2E_{66})\alpha\beta^2)c_2 \\
\mathrm{K}_{35} = \mathrm{K}_{53} &= -(E_{22}\beta^3 + (E_{12} + 2E_{66})\alpha^2\beta)c_2 \\
&\quad + \left[\left(1 - \frac{1}{3}\right)\eta h H_x^2 \alpha\right]c_1 \\
\mathrm{K}_{44} &= (F_{55} + G_{11}\alpha^2 + G_{66}\beta^2)c_2 \\
\mathrm{K}_{45} = \mathrm{K}_{54} &= (G_{12} + G_{66})\alpha\beta c_2 \\
\mathrm{K}_{55} &= (F_{44} + G_{66}\alpha^2 + G_{22}\beta^2)c_2
\end{aligned} \tag{32a}$$

$$\begin{aligned}
\mathrm{M}_{11} &= I_1 c_1 \\
\mathrm{M}_{12} = \mathrm{M}_{15} = \mathrm{M}_{51} &= 0 \\
\mathrm{M}_{13} &= -\alpha I_2 c_1 \\
\mathrm{M}_{14} = \mathrm{M}_{41} &= I_4 c_1 \\
\mathrm{M}_{21} = \mathrm{M}_{24} = \mathrm{M}_{42} &= 0 \\
\mathrm{M}_{22} &= I_1 c_1 \\
\mathrm{M}_{23} &= -\beta I_2 c_1 \\
\mathrm{M}_{25} &= I_4 c_1 \\
\mathrm{M}_{31} &= -\alpha I_2 c_1 \\
\mathrm{M}_{32} &= -\beta I_2 c_1 \\
\mathrm{M}_{33} &= I_3(\alpha^2 + \beta^2)c_1 + I_1 c_1 \\
\mathrm{M}_{34} &= -\alpha I_5 c_1 \\
\mathrm{M}_{35} &= -\beta I_5 c_1 \\
\mathrm{M}_{43} &= -\alpha I_5 c_1 \\
\mathrm{M}_{44} &= I_6 c_1 \\
\mathrm{M}_{45} = \mathrm{M}_{54} &= 0 \\
\mathrm{M}_{52} &= I_4 c_1 \\
\mathrm{M}_{53} &= -\beta I_5 c_1 \\
\mathrm{M}_{55} &= I_6 c_1 \\
c_1 &= 1 + (ea)^2(\alpha^2 + \beta^2) \\
c_2 &= 1 + l_m^2(\alpha^2 + \beta^2)
\end{aligned} \tag{32b}$$

3.3.2 Solution of transient problem of nanoplate in thermomagnetic environments under moving load

Applying the external applied moving load, the nonclassical forced vibration problem of the FGM nanoplate under thermomagnetic fields is achieved. Substituting the assumed displacements in Eq. (30) into (24) one can derive the following system of equations:

$$\mathbf{M}\ddot{\mathbf{d}} + \mathbf{K}\,\mathbf{d} = \mathbf{F}. \tag{33}$$

where F is the external force vector and it can be defined according to the type of the transverse load $q(x)$ as given below (Reddy 2007):

$$\mathbf{F} = \begin{Bmatrix} 0 \\ 0 \\ Q_{mn}c_1 \\ 0 \\ 0 \end{Bmatrix}. \tag{34}$$

The external load can be expanded in Fourier series and the term Q_{mn} is defined as follows, (Kim *et al.* 2019):

$$q(x) = \sum_m \sum_n Q_{mn} \sin(\alpha x)\sin(\beta y) \tag{35a}$$

$$Q_{mn} = \tfrac{4}{ab}\int_0^a \int_0^b q(x)\sin(\alpha x)\sin(\beta y)\,dxdy \tag{35b}$$

For point load at (x_p, y_p), the external load is defined as $q(x, y, t) = F\delta(x - x_p, y - y_p)$ and Q_{mn} is derived as:

$$Q_{mn} = \frac{4F}{ab}\int_0^a \int_0^b \sin\left(\frac{m\pi}{a}(x_p = vt)\right)\sin\left(\frac{n\pi}{b}y_p\right)dxdy, \quad m, n = 1, 3, 5, \ldots \tag{36a}$$

$$x_p, y_p = a, \frac{b}{2}, \xrightarrow{yields} Q_{mn} = \frac{4F}{ab}\sin\frac{m\pi}{2}\sin\frac{n\pi}{2}, \quad m, n = 1, 3, 5, \ldots \tag{36b}$$

For uniform load (Kim *et al.* 2019):

$$q(x) = q_0, \qquad Q_{mn} = \frac{16q_0}{mn\pi^2}, m, n = 1, 3, 5, \ldots \tag{37}$$

The following dimensionless parameters are used:

$$\lambda_{mn} = \left(\frac{\omega_{mn}a^2}{h}\right)\sqrt{\frac{\rho_m(1 - v_m^2)}{E_m}}, \qquad H_x = \frac{\varepsilon h H_x^2 a^2}{D_c}, \qquad D_c = \frac{Eh^3}{12(1 - v^2)} \tag{38}$$

Here, λ_{mn} is the frequency parameter and H_x is the magnetic field intensity parameter.

4. Numerical Results

4.1 Validation

A first comparison is made for simply supported orthotropic plates under uniform transverse load without thermal effect, using the following material properties: $E_1 = 10.94 \times 10^6$ psi, $E_2 = 20.83 \times 10^6$ psi, $G_{12} = 6.10 \times 10^6$ psi, $G_{13} = 6.19 \times 10^6$ psi, $G_{23} = 3.71 \times 10^6$ psi, $v_{12} = 0.23, v_{21} = 0.44$. Table 2 shows the comparison of the dimensionless central deflection, $\frac{\bar{P}w}{hq_0}$,

Table 2 Comparison of dimensionless central deflections of SS rectangular orthotropic plates under uniform load

a/b	h/b	(Srinivas and Rao, 1970) Exact	(Arani and Jalaei, 2017) HSDT Sinusoidal Share	(Sobhy, 2015) HSDT Two variable share	Present HSDT
0.5	0.05	2048.7	2053.4	2045.3	2048.5
	0.10	139.08	139.92	137.98	138.91
	0.14	39.790	40.226	39.297	39.612
1	0.05	10443	10459	10429	10452
	0.10	688.57	690.28	682.72	687.24
	0.14	191.07	191.77	188.01	189.45
2	0.05	21542	21567	21542	21540
	0.10	1408.5	1410.3	1404.0	1409.2
	0.14	387.23	387.84	384.67	386.62

Table 3 Comparison of frequency parameter $\lambda_{mn} = \left(\frac{\omega_{mn}a^2}{h}\right)\sqrt{\frac{\rho_m(1-v_m^2)}{E_m}}$ for Si_3N_4/SUS304 FGM plate

		(Pandey and Pradyumna, 2015)		(Huang and Shen, 2004)		Present HSDT	
	Mode	(1,1)	(1,2)	(1,1)	(1,2)	(1,1)	(1,2)
	n						
$T_0 = 300,$ $\Delta T = 0$	0.0	12.402	29.340	12.410	29.358	12.772	29.650
	0.5	8.504	20.144	8.675	20.262	8.932	20.493
	1	7.467	17.692	7.555	17.649	7.824	17.962
	2	6.707	15.890	6.777	15.809	6.963	15.945
	∞	5.377	12.756	5.405	12.602	5.690	12.958
$T_0 = 300,$ $\Delta T = 100$	0.0	12.182	28.942	12.382	29.243	12.641	29.544
	0.5	8.442	19.924	8.641	20.316	8.848	20.611
	1	7.350	17.518	7.514	17.694	7.755	17.992
	2	6.603	15.744	6.728	15.836	6.907	15.933
	∞	5.291	12.126	5.335	12.587	5.653	12.884
$T_0 = 300,$ $\Delta T = 300$	0.0	11.753	28.205	12.213	28.976	12.417	29.182
	0.5	8.095	19.506	8.425	20.099	8.665	20.386
	1	7.115	17.181	7.305	17.486	7.580	17.754
	2	6.390	15.459	6.523	15.632	6.736	15.941
	∞	5.100	12.469	5.104	12.342	5.482	12.672

($\bar{P} = 23.2 \times 10^6$psi) calculated by the present model and exact analytical results from (Srinivas and Rao 1970), and results of the HSDT from (Arani and Jalaei 2017) and (Sobhy, 2015). As seen from Table 2, the results of the proposed methodology are in good agreement with the results of various methods reported in the literature.

The second comparison is made for the FGM plate made of Si3N4/SUS304 which is previously studied by (Pandey and Pradyumna, 2015). The dimensions of the square plates are assumed as $a = b = 0.2\,m$ and $h = 0.025\,m$ and with the material properties presented in Table 1. The non-dimensional frequency parameter is defined by $\lambda_{mn} = \omega_{mn}(a^2/h)\sqrt{\rho_m(1-v_m^2)/E_m}$, $(T_0 = 300K)$. The temperature-dependent material properties are given at $T_0 = 300K$, with $\rho_m = 8166\,kg/m^3, v_m = 0.3178,\ E_m = 2.0779 \times 10^{11} Pa.$ on the other hand the temperature inside plate thickness is calculated from one dimensional heat conduction equation defined by

$$\frac{d}{dz}\left[K\frac{dT}{dz}\right] = 0, \tag{39}$$

where K is the coefficient of thermal conductivity. The developed methodology is applied to obtain the non-dimensional frequency parameter which is presented and compared with the corresponding results found in the literature as shown in Table 3. It is observed that results of the current method are in good agreement with those of finite element formulation (Pandey and Pradyumna 2015) and analytical solution (Huang and Shen 2004).

4.2 Free vibration response

For the free vibration behaviour of the FGM nanoplate, a simply supported small-scale square plate, with the dimensions $a = b = 100\,nm, h = a/10$, otherwise stated and made of ceramic (Silicon nitride: Si_3N_4) and metal

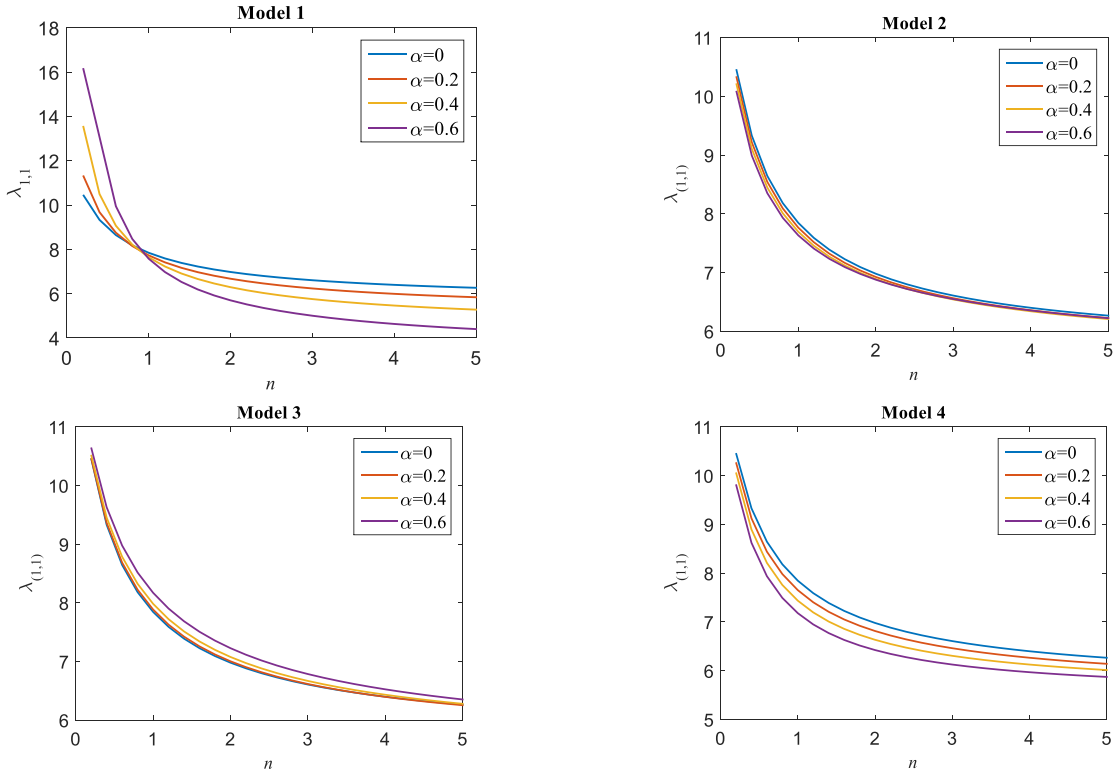

Fig. 3 Variation of the dimensionless frequency $\lambda_{(1,1)}$ with the material gradation index n between 0.2 to 5 and porosity index $= 0.0,\ 0.2,\ 0.4$ and 0.6 , nonlocal parameter $e_0a = 0$ and material size factor $l_m = 0$, temperature rise $\Delta T = 0$, Magnetic field intensity $H_x = 0$

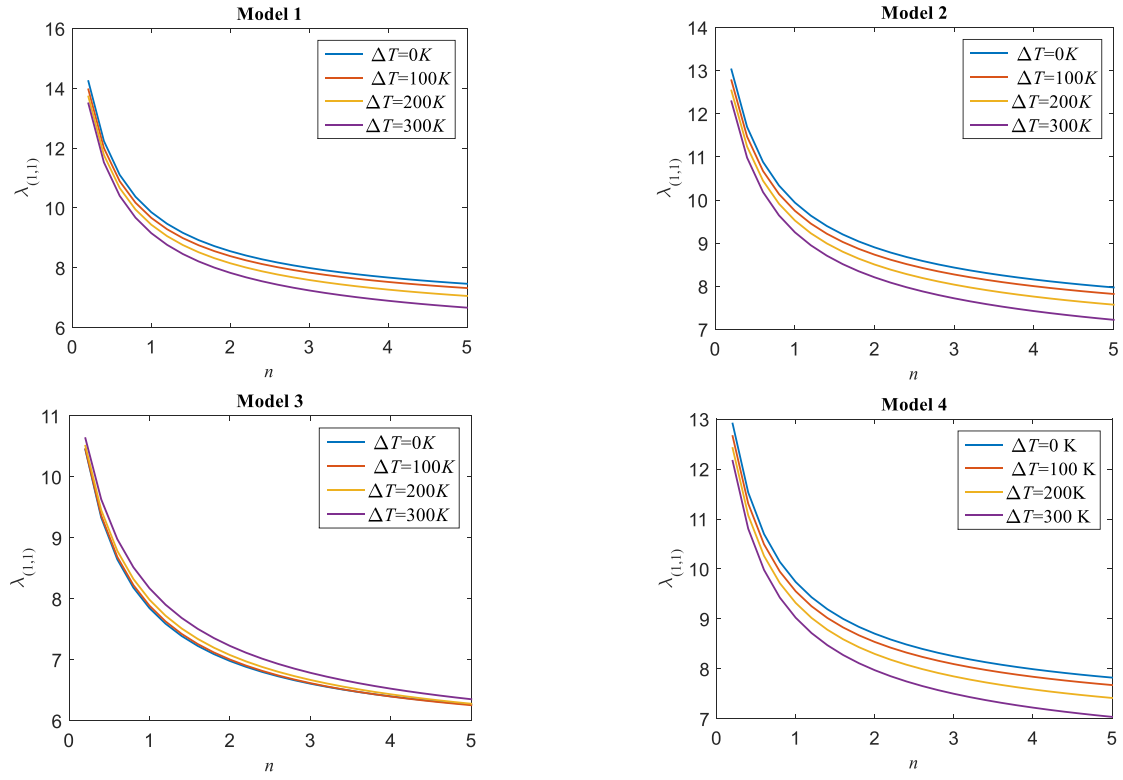

Fig. 4 Considering different models, variation of the dimensionless frequency $\lambda_{(1,1)}$ depending on the material gradation index n between $0.2 - 5$ and $\Delta T = 0, 100, 200\ and\ 300\ K$, for porosity index $\alpha = 0.25, a/h = 10$, $e_0a = l_m = H_x = 0$

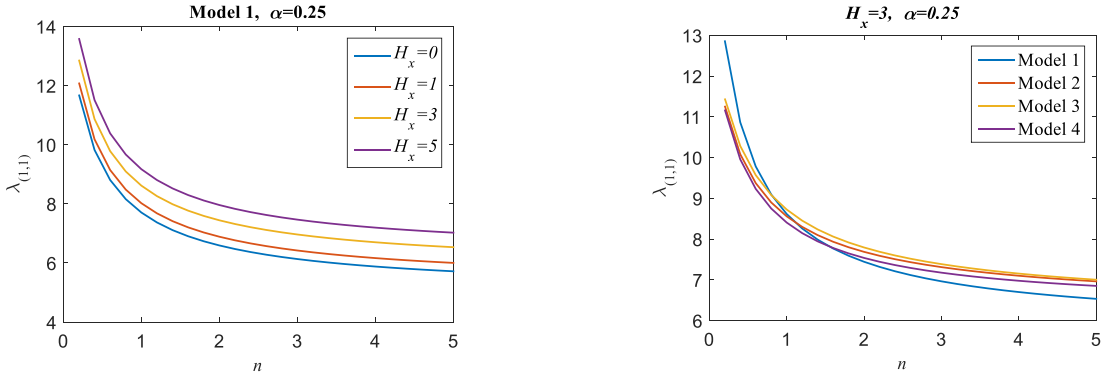

(a) (b)

Fig. 5 Considering different models, variation of the dimensionless frequency $\lambda_{(1,1)}$ depending on the material gradation index n between $0.2-5$ and magnetic field intensity $H_x = 0, 1, 3\ and\ 5$, for porosity index $\alpha = 0.25, a/h = 10$, $e_0a = l_m = \Delta T = 0$

(Stainless steel: SUS304) with the temperature-dependent material properties given in Table 2, is considered. The frequencies ω_{mn} for the modes (m,n) are calculated using the eigen value problem defined by Eq. (31). The dimensionless frequency parameters are obtained with $\lambda_{mn} = \omega_{mn}(a^2/h)\sqrt{\rho_m(1-v_m^2)/E_m}$ in which ρ_m, v_m and E_m are the material properties of the metal constituent at room temperature.

Considering the different porosity models, Fig. 3 shows variations of the dimensionless frequency $\lambda_{(1,1)}$ with the material grading index *n* for the porosity volume fractions of α=0.0, 0.2, 0.4 and 0.6. Here, the non-local parameter, material size parameter, temperature rise, and magnetic field intensity are zero. As can be seen from the figures, the fundamental frequency declines sharply for $n \leq 2$, and after that, the declining tendency slows down and approaches the limit for larger values, i.e., n>4. This means that the metal constituent is higher, and the entire composition tends towards a metal homogeneous structure. As the stiffness of the plate decreases at large values of the grading index, the frequency parameters will also decrease, and the general trends of the frequency profiles show this. In comparison, the tendency to approach the limit state in models 1 and 4 is seen at lower *n* values than in models 2 and 3. Moreover, increasing the material porosity index, α results in more decrease in the dimensionless frequency parameters for porosity distribution models 1, 2, and 3 while this trend is reversed for model 4. This due to the decrease in the ratio of the equivalent material stiffness to the equivalent inertia.

Keeping constant value of the material porosity index $\alpha = 0.25$ and aspect ratio, $a/h = 10$ and incorporating the thermal effect, Fig 4 shows the frequency variations depending on material gradation index and temperature rise for $e_0a = l_m = H_x = 0$. When the material composition is rich in ceramics, i.e., $n \leq 1$, the effect of temperature rise is small because of the better temperature behaviour of the ceramic in the composition. However, for all models, the increase in the metal constituent rapidly decreases the frequencies, because of the softening effect associated with the thermal effect, as well as the lower strength compared to the ceramic-weighted composition. In Model 4, where the pores are concentrated close to the upper surface, a faster decrease in frequencies is seen compared to the others due to the increase in temperature.

Neglecting the thermal effect and introducing the magnetic effect, Fig. 5a shows the frequency variations versus *n* for different horizontal magnetic field intensities H_x=0,1, 3, 5 and a fixed porosity index, α, where $\alpha = 0.25$, and $a/h = 10$, $e_0a = l_m = \Delta T = 0$. While Fig. 5b depicts the comparisons of the porosity models for the same magnetic field intensity $H_x = 3$. As seen in the figures, unlike the temperature rise, the magnetic field intensity increases the frequencies due to the associated stiffening effect. This means that the vibration stability of a nanoplate in a thermal field can be enhanced and controlled using a directed magnetic field, and this effect of the magnetic field could be beneficial for the application and design of NEMS (Jalaei and Arani, 2018, Jalaei and Thai, 2019). It can be also seen that, keeping constant value of the porosity index, Porosity distribution model 1 results in more rapid decrease in the dimensionless frequency parameter with *n* while model 3 produces slower decreasing rate.

Introduction of the nonlocal effect in the absence of the microstructure effect, considering the uniform porosity distribution model, Fig. 6a shows the frequency variations for several nonlocal parameters of e_0a=0, 1, .2 and 4 nm with the material grading index *n*. While Fig. 6b presents a comparison of the results of the porosity models for a constant nonlocal parameter value of 2 nm. In all analyses, the porosity index is α=0.25 and the other parameters are zero. Due to the softening effect on the nanoplate (Eringen, 1983), the increase of the nonlocal parameter decreases the dimensionless frequencies. Comparison between the considered porosity distribution models shows that rapid decrease in the dimensionless frequencies are obtained with model 1 while model 3 results in slower decrease in the dimensionless frequencies with the material grading index.

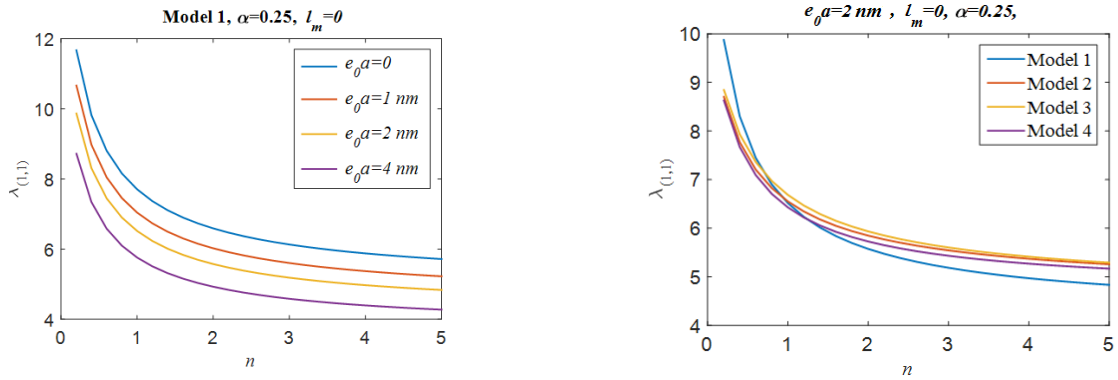

(a) (b)

Fig. 6 Considering different models, variation in the dimensionless frequency $\lambda_{(1,1)}$ depending on the material gradation index n between $0.2-5$ and nonlocal parameter $e_0a = 0, 1, 2\ and\ 4\ nm$, for porosity index $\alpha = 0.25, a/h = 10$, $l_m = \Delta T = H_x = 0$

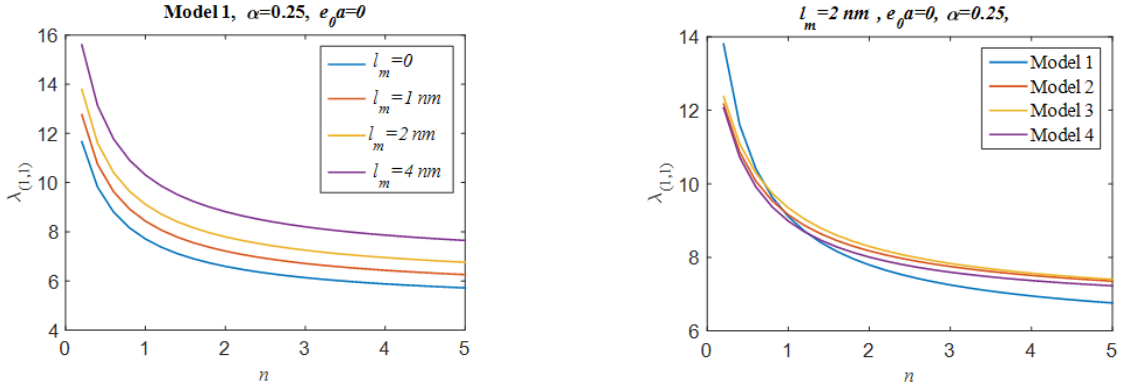

(a) (b)

Fig. 7 Considering different models, variation of the dimensionless frequency $\lambda_{(1,1)}$ depending on the material gradation index n between $0.2-5$ and material size factor $l_m = 0, 1, 2\ and\ 4\ nm$, for porosity index $\alpha = 0.25, a/h = 10$, $e_0a = \Delta T = H_x = 0$

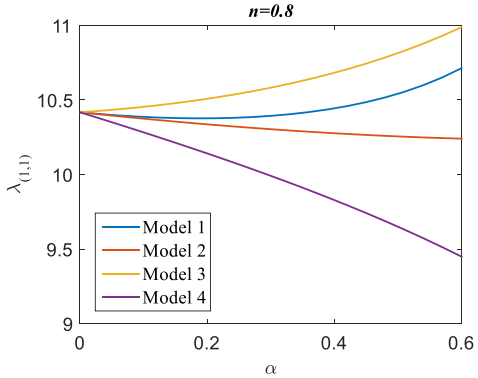

Fig. 8 Variation of the dimensionless frequency $\lambda_{(1,1)}$ depending on the porosity distribution and porosity index α between $0.0-0.6$, for $n = 0.8$ and $a/h = 10$, $e_0a = l_m = \Delta T = H_x = 0$

On the other hand, neglecting the nonlocality effect and incorporating the material size effect leads to stiffening effect, as witnessed in Fig 7. Due to this stiffening effect of the material size parameter the dimensionless frequencies increase with increasing the material size parameter (Lim *et al.* 2015). It is important to indicate that for good comparison, values of both nonlocal and size parameters are assumed as the same in this study, but they may differ. The real values of these can be described by molecular dynamics simulations (Giannopoulos *et al.* 2008) and experimental studies (Li and Hu 2016).

Keeping constant value of the material grading index,

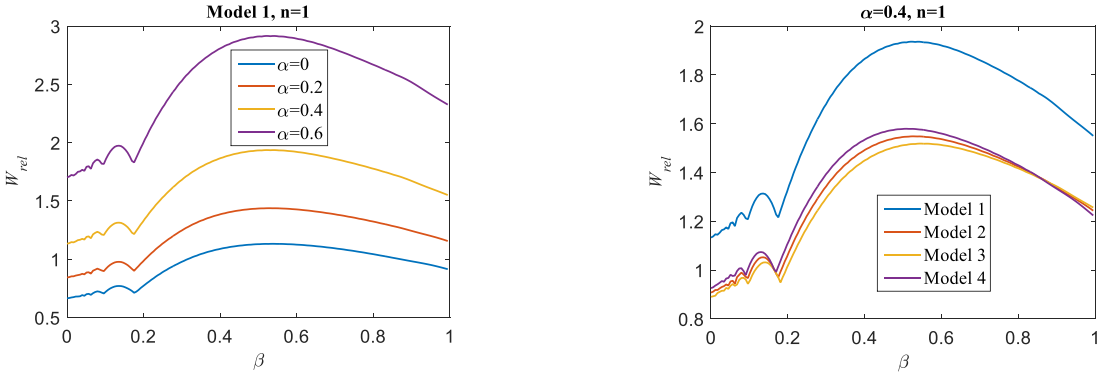

(a) (b)

Fig. 9 a) Comparisons of maximum mid-span deflections of FG nanoplate versus speed parameter β and porosity distribution, for porosity index $\alpha = 0.0, 0.2, 0.4, 0.6$, material gradation index $n = 1$ and aspect ratio $a/h = 10$, nonlocal parameter, material size parameter, temperature rise, and magnetic field intensity, respectively are: $e_0a = l_m = \Delta T = H_x = 0$. b) Comparisons of different porosity models for $\alpha = 0.4$

Fig. 8 shows the effect of the porosity distribution models and the material porosity index between $\alpha = 0.0 - 0.6$ on the frequency variations for $n = 0.8, a/h = 10$, $e_0a = l_m = \Delta T = H_x = 0$. For the chosen material composition, the effects of the porosity index are different depending on the porosity distribution model. It is noticed that in the uniform and asymmetric bottom surface concentrated distributions, the frequencies rise with the increasing porosity index. On the contrary, in the symmetric and top surface concentrated porosity distributions, these frequencies are decreased with increasing the material porosity index.

4.3 Forced vibration response to moving load

The proposed numerical method is applied to analyze the forced vibration response of functionally graded simply supported porous FGM nanoplates under a moving load. The Newmark numerical integration method is applied to solve the forced motion Eq. (33) using $\Delta t = T_{final}/500, T_{final} = L/v$. In the analysis, the moving load is chosen as $1\,nN$. The dimensionless speed parameter, β is utilized as $\beta = v/v_{crital}$, when β=1 indicates the load velocity is equal to the first critical speed of the plate, where $v_{critical} = \omega_{(1,1)}a/\pi$ (Frýba, 1999). A dimensionless displacement adopted here with $W_{rel} = \frac{W(a/2,b/2,t)}{W_{static}(a/2,b/2)|_{n=\infty}}$ by normalizing the mid-point dynamic displacements with the static mid-point displacement of the nanoplate made of pure metal.

First, the effect of the porosity volume fraction (porosity index) is examined, and in Fig. 9a, comparisons of the analysis results for the velocity parameters between β=0-1 are presented. The result of the analysis is presented for the porosity index α=0, 0.2, 0.4, 0.6 and the material grading index, n=1. The non-local parameter, material size parameter, temperature rise, and magnetic field strength values are kept as zero. ($e_0a = l_m = \Delta T = H_x = 0$). While Fig. 9b shows a comparison of different porosity models for a porosity index value of α=0.4. As can be seen from the figures, both the rise in porosity volume fraction and the distribution function impacts the dynamic behavior of the nanoplate, consequently with increasing porosity, the plate weakens, and the dynamic displacements (Fig. 9a: in uniform distribution) increase. Also the porosity distribution model (Fig. 9b), significantly affects both the dynamic response and behavior of the nanoplate. This is because the variation in the stiffness of the nanoplate causes the displacements to increase or decrease. Also variation of the natural frequency of the nanoplate significantly affects its dynamic behavior. Thus, in Fig. 9b the velocity at which the maximum displacements occur varies mainly due to the natural frequency variations according to the porosity distribution model. On the other hand, in Fig. 9b, approximately 10% more dynamic displacement arises in uniform porosity distribution than other distributions.

Introduction of the thermal effect, Fig. 10 shows the effect of temperature rise on the forced dynamic behavior of the nanoplate under moving load. Here, analyzes are performed at temperature variations of ΔT=0,100, 200 and 300 K for porosity index α= 0.25 and material gradation index n=1, and for the zero value of the nonlocal parameter, the size parameter and the magnetic field intensity. Here, Fig. 10a shows the effect of different values temperature rise for the uniform porosity distribution in model, 1, while Fig. 10b depicts a comparison of all porosity distribution models for ΔT=200 K. As seen in Fig. 10(a), the normalized dynamic displacements increase with increasing temperature rise due to increasing the material relaxation effect associated with temperature rise. Additionally the velocities at which the maximum value of the normalized dynamic displacement occur shift to the left, as can be seen in the result curves. And it is also seen that the maximum point in the curves shifts to the right or left according to the porosity model, as depicted in Fig.10b. Since both the temperature

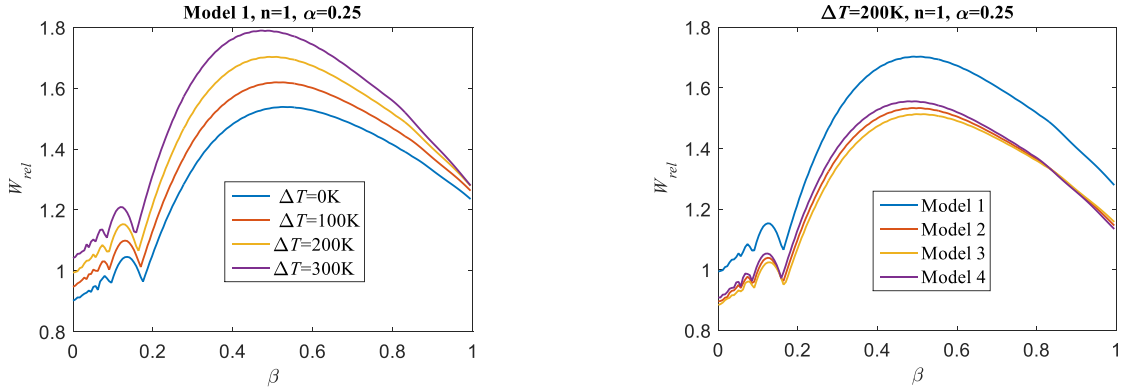

(a) (b)

Fig. 10 a) Comparisons of maximum mid-span deflections of FG nanoplate versus speed parameter β and temperature rise, for $\Delta T = 0, 100, 200\ and\ 300K$ and porosity index $\alpha = 0.25$, $n = 1$, $a/h = 10$, $e_0 a = l_m = H_x = 0$. b) Comparisons of different models for $\Delta T = 200\ K$

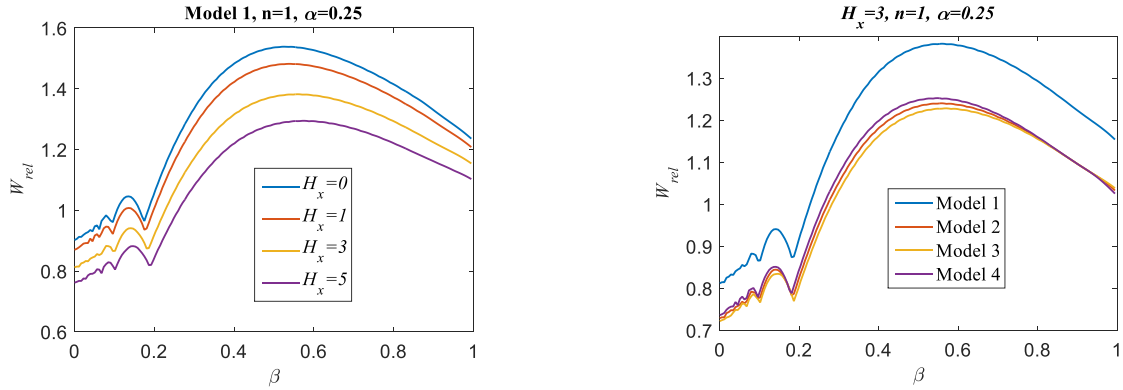

(a) (b)

Fig. 11 a) Comparisons of maximum mid-span deflections of FG nanoplate versus speed parameter β and magnetic field intensity for $H_x = 0, 1, 3\ and\ 5$, and porosity index $\alpha = 0.25$, $n = 1$, $a/h = 10$, $e_0 a = l_m = \Delta T = 0$. b) Comparisons of different models for $H_x = 3$

rise and the porosity distribution function affect the forced dynamic behavior of the nanosplate, the responses are accordingly different.

Considering the influence of the magnetic field intensity on the forced dynamic behavior of nanoplate, Fig. 11a, shows the normalized dynamic displacement profiles with the normalized velocity at different values of the magnetic field intensity. Here, according to Eq. (38), the magnetic field strength is taken as dimensionless values of H_x=0, 1, 3, 5. On the other hand, Fig.11b, illustrates comparisons of dynamic responses of all porosity distribution models for a fixed value of H_x=3. In all analyses, the porosity index α=0.25 and the material gradation index n=1 is fixed. It can be seen that the magnetic field intensity produces stiffening effect which results in decreasing the normalized dynamic displacements of the nanoplate. This is due to the fact that the Lorentz force induced by the magnetic field resists the motion of the nanoplate. Thus, this effect of this force can reduce the displacements caused by the temperature rise (as depicted Fig. 10).

Fig. 12a shows the normalized dynamic displacements of the porous nanoplate regarding the variation of the material grading index (n=0, 1, 2, 10). While Fig. 12b is a comparison of the dynamic responses of different porosity distribution models for a fixed material grading index n=2. Where the porosity index is α=0.25 and the temperature rise, magnetic field strength, and non-local effects are kept as zero in all analyzes. The full-ceramic structure, which appears as a blue curve in Fig. 12a, with n=0, the maximum of the normalized dynamic displacement is seen at the value of velocity parameter β=1. This is the smallest one of the maximum displacements in the curves, since the entire structure is ceramic, n=0. When the metal constituent is increased (Fig. 12a) with increasing the material gradation index, n, this causes an increase in response and a change in vibration behavior since the dimensionless velocity value at which the maximum normalized displacement occurs in the curves shifts to the left. For example, at n=0 the maximum occurs at β=1, while at n=10 the maximum occurs at β=0.35. This shift is directly related to the change in the

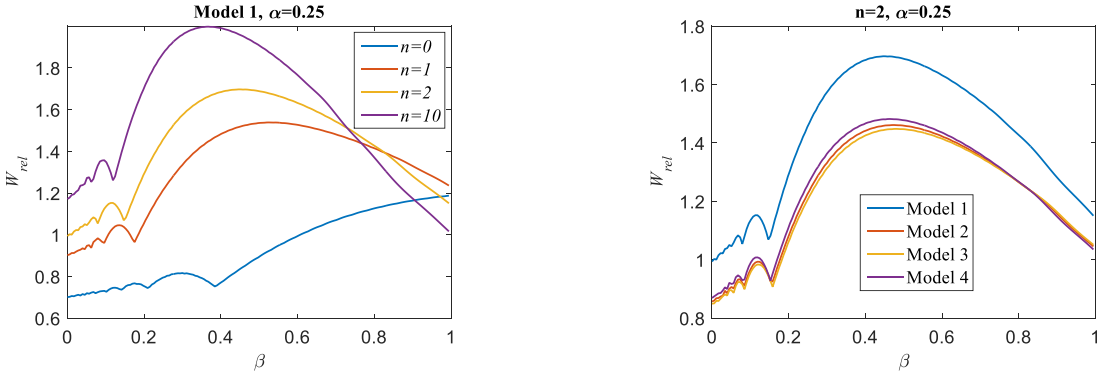

(a) (b)

Fig. 12 a) Comparisons of maximum mid-span deflections of FG nanoplate versus speed parameter β and material gradation index for $n = 0, 1, 2\ and\ 10$ and porosity index $\alpha = 0.25,\ a/h = 10,\ e_0a = l_m = H_x = \Delta T = 0$. b) Comparisons of different models for $n = 2$

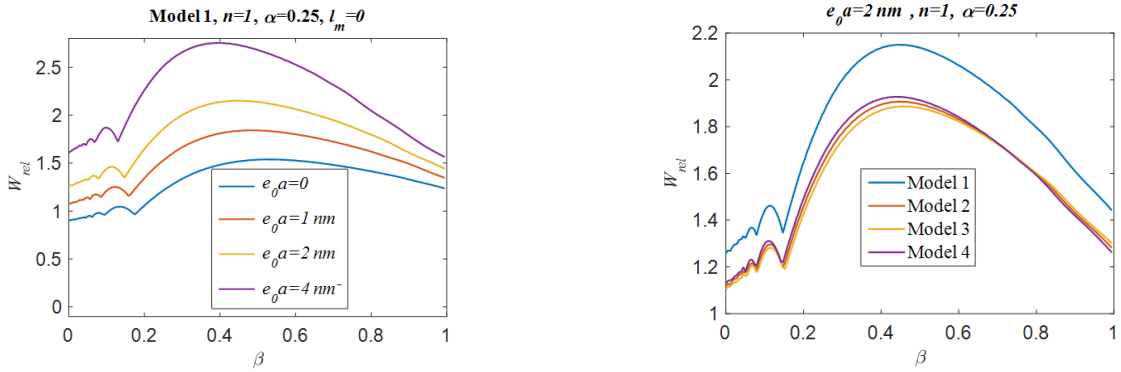

(a) (b)

Fig. 13 a) Comparisons of maximum midspan deflections of FG nanoplate versus speed parameter β and nonlocal parameter for $e_0a = 0, 1, 2and\ 4\ nm^2$ and $n = 1, \alpha = 0.25,\ a/h = 10,\ l_m = H_x = \Delta T = 0$. b) Comparisons of different models for $e_0a = 2\ nm$

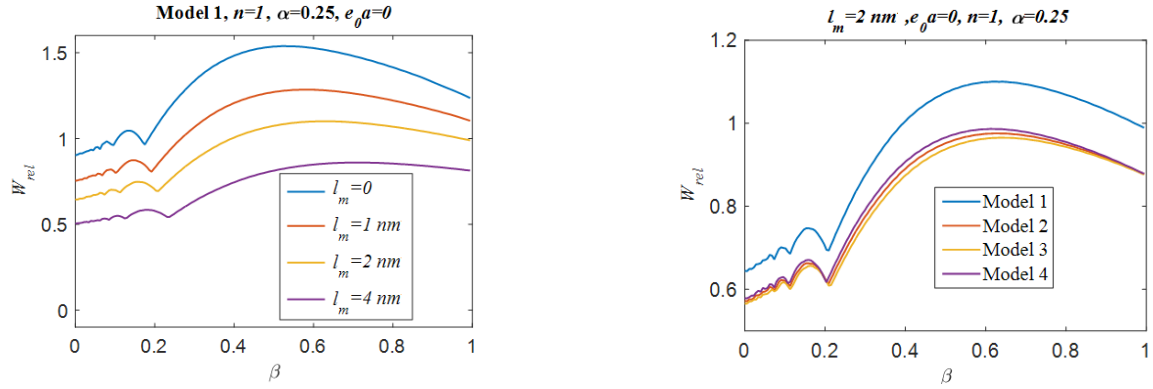

(a) (b)

Fig. 14 a) Comparisons of maximum midspan deflections of FG nanoplate versus speed parameter β and size parameter for $l_m = 0, 1, 2and\ 4\ nm$ and $n = 1, \alpha = 0.25,\ a/h = 10,\ e_0a = H_x = \Delta T = 0$. b) Comparisons of different models for $l_m = 2\ nm$

natural frequencies of the nanoplate because of the change in material composition. It is better to mention here that, at the maximum response the critical load speed is reached where $v_c=\omega\pi/a$, and $\beta=\omega/\omega_{(1,1)}=1$, $\omega=\pi v/a$, with ω refers to excitation frequency of the load (Frýba, 1999, Oguamanam *et al.* 1998).

The normalized dynamic displacements of the nanoplate according to the change of the non-local parameter are given in Fig. 13a, assuming fixed α=0.25 and n=1, and $e_0a = l_m = \Delta T = H_x = 0$. While Fig. 13b presents the

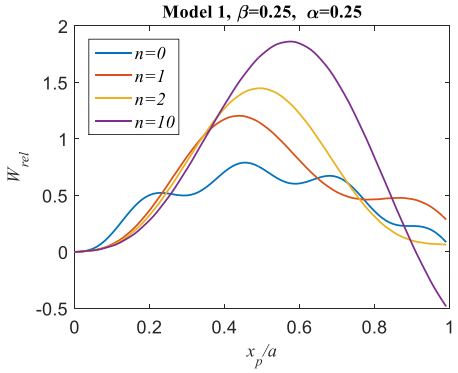

(a)

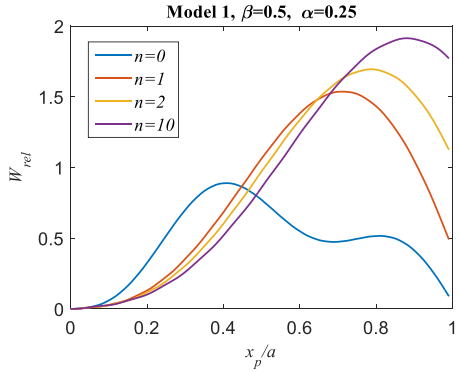

(b)

Fig. 15 Comparisons of time histories of midpoint deflections of FG nanoplate for β =0.25 and 0.5 and $n = 0, 1, 2, 10$ and $\alpha = 0.25$, $a/h = 10$, $e_0a = l_m = H_x = \Delta T = 0$

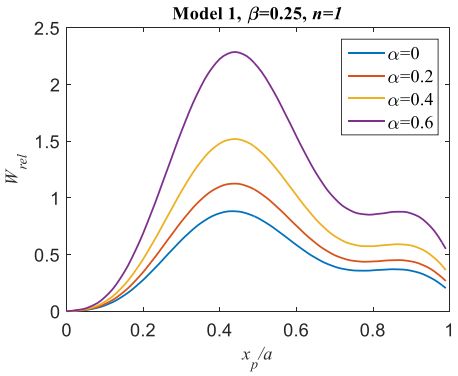

(a)

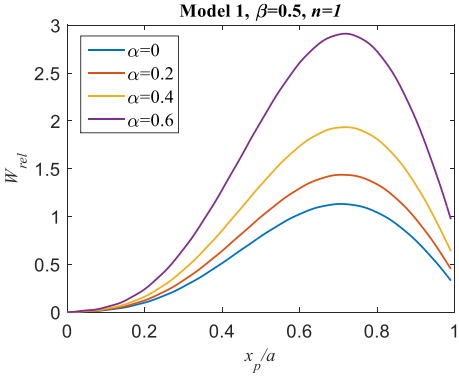

(b)

Fig. 16 Comparisons of time histories of midpoint deflections of FG nanoplate for β =0.25 and 0.5 and $\alpha = 0, 0.2, 0.4, 0.6$ and $n = 1$, $a/h = 10$, $e_0a = l_m = H_x = \Delta T = 0$

comparative dynamic responses of the nanoplate for all porosity distribution models with a non-local parameter of $e_o a$=2 nm. As seen in Fig. 13a, the normalized dynamic displacements increase because of the softening in the nanoplate depending on the growth in the non-local parameter, and the load velocity values at which the maximum normalized dynamic displacement occurs goes to the left.

The normalized dynamic displacements of the nanoplate according to the change of the material size parameter are given in Fig. 14a, while in Fig. 14b, the dynamic responses of all porosity distribution models are given comparatively for the fixed value of the material size parameter of l_m=2 nm and others are taken as in Fig. 13. As seen in Fig. 14a, the normalized dynamic displacements decrease with increasing the material size parameter due to the effect of rising rigidity in the nanoplate with the growth in the material size parameter. Moreover, the velocity values at which resonance occurs move to the right, since the increasing size parameter increases the load velocity at which maximum response occurs.

The dynamic behavior of the porous nanoplate is well understood from the time-dependent vibrational behavior. In Fig. 15, depending on the material composition, the time-dependent dynamic responses of the uniform porosity model for the constant porosity index α=0.25 are presented comparatively for the velocity parameters β=0.25 and 0.50. Here, non-local effects, temperature rise, and magnetic field are considered zero. In the figures, the horizontal axis shows the dimensionless position x_p/a of the load on the plate in the range 0-1, and at a zero value of the dimensionless position, the load is at the left end of the plate and a value of 1 means that it reaches the right end. As can be seen from the analysis, results performed at the velocity parameter β=0.25 given in Fig. 15a, at n=0 (full-ceramic) the nanoplate has completed four full-periods of vibration (four full sine waves), whereas at n=10 (almost full-metal) it is seen that the nanoplate has completed only almost as a half-sine wave of vibration. If an exact half-sine wave occurs in the vibration, it means that it has reached the critical velocity for the chosen material composition. On the right in Fig. 15b, the analysis results with velocity parameter β=0.5 show that the time-dependent vibration is slightly larger than a 1.5 sine wave at n=0 and a quarter sine wave at n=10. These results are in good agreement with the reported ones by (Frýba 1999, Oguamanam *et al.* 1998)

Fig. 16 presents the analysis results for α=0, 0.2, 0.4, and 0.6 values of the porosity index and the values of the β=0.25 and 0.5 in the uniform porosity model. According to the figures, the normalized dynamic displacements increase

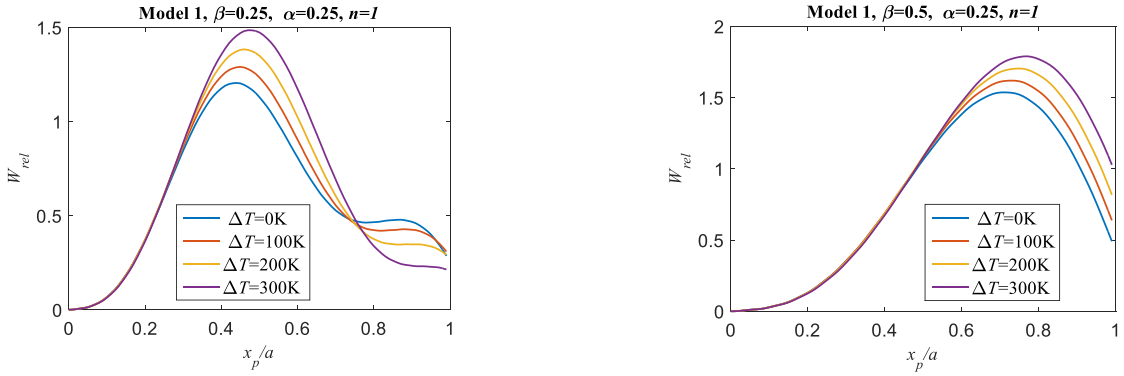

(a) (b)

Fig. 17 Comparisons of time histories of midpoint deflections of FG nanoplate for β =0.25 and 0.5 and $\Delta T = 0, 100, 200, 300\ K$ and $\alpha = 0.25,\ n = 1\ \ a/h = 10,\ e_0 a = l_m = H_x = 0$

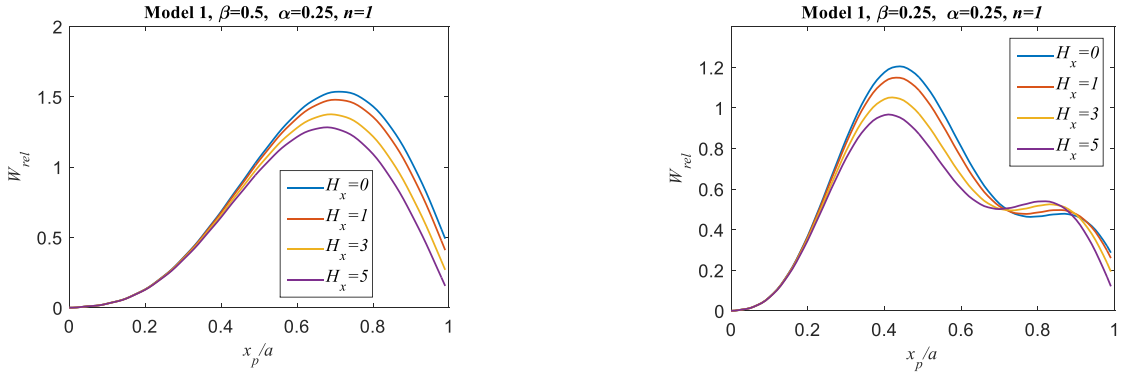

(a) (b)

Fig. 18 Comparisons of time histories of midpoint deflections of FG nanoplate for β =0.25 and 0.5 and $H_x = 0, 1, 3, 5$ and $\alpha = 0.25,\ n = 1,\ a/h = 10,\ e_0 a = l_m = \Delta T = 0$

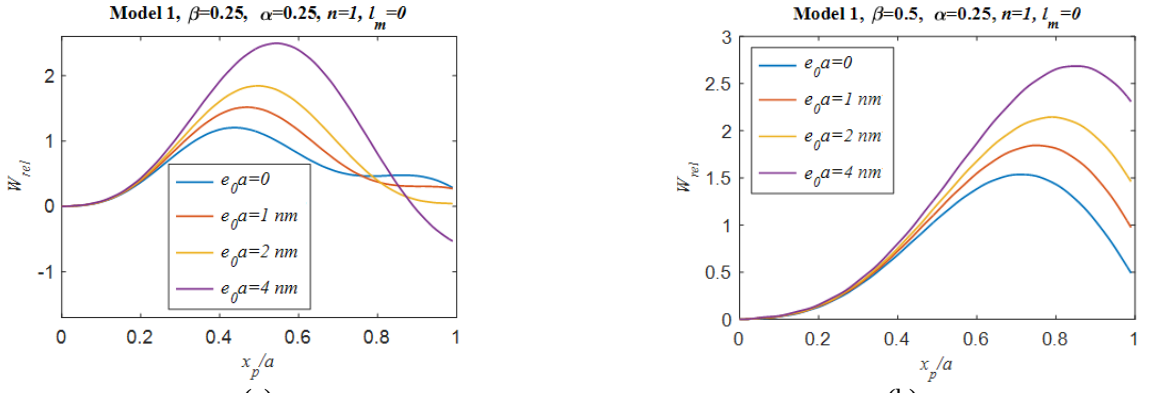

(a) (b)

Fig. 19 Comparisons of time histories of midpoint deflections of FG nanoplate for β =0.25 and 0.5 and $e_0 a = 0, 1, 2, 4\ nm$ and $\alpha = 0.25,\ n = 1,\ a/h = 10,\ l_m = H_x = \Delta T = 0$

because of the weakening in the nanoplate stiffness caused by the growth in the porosity index, but the vibrational behavior of the nanoplate shifts little with the growth in the porosity index. This appears as a blue curve representing the change of fundamental frequency depending on the porosity index in Fig. 8 for a uniform porosity distribution.

Fig. 17 presents the analysis results for the uniform porosity model at ΔT=0, 100, 200, and 300 K temperature growth and the velocity parameters at β=0.25 and 0.5. According to the figures, the normalized dynamic displacements increase because of the material relaxation due to thermal effect which results in decreasing the nanoplate stiffness, and the vibration behavior of the nanoplate changes depending on the temperature rise. Additionally, depending on the increasing temperature, the wavenumber of the time-dependent vibration decreases.

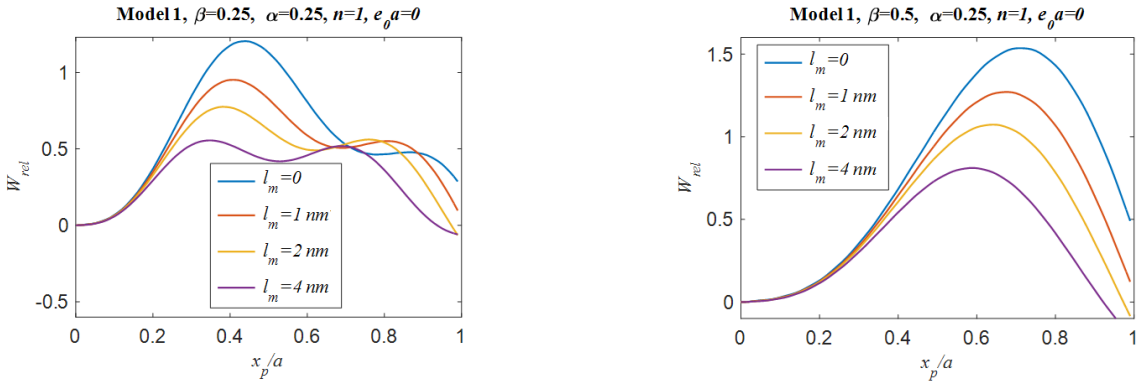

(a) (b)

Fig. 20 Comparisons of time histories of midpoint deflections of FG nanoplate for β =0.25 and 0.5 and $l_m = 0, 1, 2, 4\ nm$ and $\alpha = 0.25,\ n = 1,\ a/h = 10,\ e_0a = H_x = \Delta T = 0$

Fig. 18 shows the time-dependent vibrations of the nanoplate depending on the dimensionless magnetic field intensity. Here, the porosity index is taken as α=0.25 and material gradation index is n=1, and the analyses are performed at values of the velocity parameter, β=0.25 and 0.5. It is understood from the curves in the figure that the increase in the intensity of the magnetic field reduces the forced vibration responses of the nanoplate, in contrast to the temperature rise, as depicted Fig. 17.

Fig. 19 presents the time-dependent vibration responses of the nanoplate depending on the nonlocal parameter. While Fig. 20 shows the effect of the material size parameter when the nonlocal parameter is kept zero. It can be seen that incorporation of the nonlocality effect produces softening effect of the nanoplate which results in larger values of the normalized dynamic displacements with increasing the nonlocal parameter, as illustrated in Fig. 19. On the contrary, introduction of the material size parameter leads to stiffening effect which results in enhancement of the nanoplate stiffness thus smaller values of the normalized dynamic displacements are detected with increasing the material parameter, as seen in Fig. 20.

5. Conclusions

In this study, the nonclassical electromagnetic free and forced vibration behaviors of a porous FGM nanoplate are studied and analyzed using the HSDT and NGST. The nanoplate is exposed to a moving load in thermal and magnetic environments. The porosity distributions in the nanoplate is examined using four different distribution models. Uniform, symmetrical, asymmetric up and bottom distribution models are used and compared. The system of equations of motion are derived based on the Hamilton principle and solved analytically using the Navier method. Numerical results are obtained and discussed. The factors affecting the dynamic behavior of the FGM porous nanoplate are analyzed separately and the following concluding remarks are recorded:

• The actual natural frequency of nanoplate is effective in the dynamic behaviour. It is dependent on several parameters, temperature change, material composition, microstructure size and nonlocal parameters, the volume fraction of porosity, and distribution function of porosity.

• Incorporating thermal effect produces material relaxation which results in decreasing the resonant frequencies and producing larger values of the normalized dynamic displacements with increasing temperature. This effect is dependent on the porosity distribution function.

• On the contrary, introduction of the magnetic effect results in stiffening effect. Increasing the magnetic field intensity leads to increasing the resonant frequencies and decreasing the normalized dynamic displacement. Thus, this effect of the magnetic field can be used to dampen the vibrations of nanoplates exposed to harsh conditions such as temperature rise and a moving load.

• The porosity and its distribution throughout the nanoplate thickness significantly affect the free and forced vibration behaviour of the nanoplate. Dynamic behaviour could be controlled by selecting appropriate value of the porosity parameter and suitable porosity distribution model.

• The material composition in the nanoplate significantly affects the dynamic behaviour of the nanoplate.

• The nonlocal parameter causes the nanoplate to behave softer, and the material microstructure size parameter, on the contrary, causes it to behave stiffer.

• The maximum response occurs at the load speed where the influence frequency of the moving load and the fundamental frequency of the nanoplate in the selected properties are the same.

• The current study could be extended to study the nonclassical dynamic behaviour of porous viscoelastic functionally graded nanoplate in thermomagnetic environments under moving load.

Acknowledgments

This research work was funded by Institutional Fund Projects (grant no. IFPIP: 206-135-1442). The authors gratefully acknowledge the technical and financial support from the Ministry of Education and King Abdulaziz University, DSR, Jeddah, Saudi Arabia.

References

Aghababaei, R. and Reddy, J.N. (2009), "Nonlocal third-order shear deformation plate theory with application to bending and vibration of plates", *J. Sound Vib.*, **326**, 277-289. https://doi.org/10.1016/j.jsv.2009.04.044

Akavci, S.S. (2014), "An efficient shear deformation theory for free vibration of functionally graded thick rectangular plates on elastic foundation", *Compos. Struct.*, **108**, 667-676. https://doi.org/10.1016/j.compstruct.2013.10.019

Alazwari, M.A., Esen, I., Abdelrahman, A.A., Abdraboh, A.M. and Eltaher, M.A. (2022), "Dynamic analysis of functionally graded (FG) nonlocal strain gradient nanobeams under thermo-magnetic fields and moving load", *Adv. Nano Res.*, **12**(3), 231-251. https://doi.org/10.12989/anr.2022.12.3.231

Ansari, R., Ashrafi, M.A., Pourashraf, T. and Sahmani, S. (2015), "Vibration and buckling characteristics of functionally graded nanoplates subjected to thermal loading based on surface elasticity theory", *Acta Astronaut.*, **109**, 42-51. https://doi.org/https://doi.org/10.1016/j.actaastro.2014.12.015

Arani, A.G. and Jalaei, M.H. (2017), "Investigation of the longitudinal magnetic field effect on dynamic response of viscoelastic graphene sheet based on sinusoidal shear deformation theory", *Physica B*, **506**, 94-104. https://doi.org/10.1016/j.physb.2016.11.004

Askari, M., Brusa, E. and Delprete, C. (2021), "On the vibration analysis of coupled transverse and shear piezoelectric functionally graded porous beams with higher-order theories", *J. Strain Anal. Eng.*, **56**, 29-49. https://doi.org/10.1177/0309324720922085

Azartash, P., Khorsandijou, S.M. and Khorshidvand, A.R. (2021), "Enhanced geometrically-nonlinear poro-FG shear-deformable beams under moving load in discrete state-space", *Austral. J. Mech. Eng.*, 1-28. https://doi.org/10.1080/14484846.2021.1914389

Bendaho, B., Belabed, Z., Bourada, M., Benatta, M.A., Bourada, F. and Tounsi, A. (2019), "Assessment of new 2D and quasi-3D Nonlocal theories for free vibration analysis of size-dependent functionally graded (FG) nanoplates", *Adv. Nano Res.*, **7**(4), 277-292. https://doi.org/10.12989/anr.2019.7.4.277

Boggarapu, V., Gujjala, R., Ojha, S., Acharya, S., Chowdary, S. and Kumar Gara, D. (2021), "State of the art in functionally graded materials", *Compos. Struct.*, **262**, 113596. https://doi.org/10.1016/j.compstruct.2021.113596

Chen, D., Yang, J. and Kitipornchai, S. (2016), "Free and forced vibrations of shear deformable functionally graded porous beams", *Int. J. Mech. Sci.*, **108-109**, 14-22. https://doi.org/10.1016/j.ijmecsci.2016.01.025

Chen, D., Zheng, S., Wang, Y., Yang, L. and Li, Z. (2020), "Nonlinear free vibration analysis of a rotating two-dimensional functionally graded porous micro-beam using isogeometric analysis", *Eur. J. Mech. A Solids*, **84**, 104083. https://doi.org/10.1016/j.euromechsol.2020.104083

Chinh, T.H., Tu, T.M., Duc, D.M. and Hung, T.Q. (2021), "Static flexural analysis of sandwich beam with functionally graded face sheets and porous core via point interpolation meshfree method based on polynomial basic function", *Arch. Appl. Mech.*, **91**, 933-947. https://doi.org/10.1007/s00419-020-01797-x

Dang, V.H. and Do, Q.C. (2021), "Nonlinear vibration and stability of functionally graded porous microbeam under electrostatic actuation", *Arch. Appl. Mech.*, **91**, 2301-2329. https://doi.org/10.1007/s00419-021-01884-7

Derikvand, M., Farhatnia, F. and Hodges, D.H. (2021), "Functionally graded thick sandwich beams with porous core: Buckling analysis via differential transform method", *Mech. Based Des. Struct. Mach.*, 1-28. https://doi.org/10.1080/15397734.2021.1931309

Doan, T.L., Le, P.B., Tran, T.T., Trai, V.K. and Pham, Q.H. (2021), "Free vibration analysis of functionally graded porous nanoplates with different shapes resting on elastic foundation", *J. Appl. Comput. Mech.*, **7**, 1593-1605. https://doi.org/10.22055/jacm.2021.36181.2807

Ebrahimi, F., Dabbagh, A. and Taheri, M. (2021), "Vibration analysis of porous metal foam plates rested on viscoelastic substrate", *Eng. Comput.*, **37**(4), 3727-3739. https://doi.org/10.1007/s00366-020-01031-w.

Ebrahimi, F., Ghasemi, F. and Salari, E. (2016), "Investigating thermal effects on vibration behavior of temperature-dependent compositionally graded Euler beams with porosities", *Meccanica*, **51**, 223-249. https://doi.org/10.1007/s11012-015-0208-y

Ebrahimi, F. and Jafari, A. (2016), "A higher-order thermo-mechanical vibration analysis of temperature-dependent FGM beams with porosities", *J. Eng.*, **2016**, 20. https://doi.org/10.1155/2016/9561504

Eltaher, M.A., Abdelrahman, A.A., Al-Nabawy, A., Khater, M. and Mansour, A. (2014), "Vibration of nonlinear graduation of nano-Timoshenko beam considering the neutral axis position", *Appl. Math. Comput.*, **235**, 512-529. https://doi.org/10.1016/j.amc.2014.03.028.

Eltaher, M.A., Almalki, T.A., Ahmed, K.I. and Almitani, K.H. (2019), "Characterization and behaviors of single walled carbon nanotube by equivalent-continuum mechanics approach", *Adv. Nano Res.*, **7**(1), 39. https://doi.org/10.12989/anr.2019.7.1.039

Eltaher, M.A., Khater, M.E., Park, S., Abdel-Rahman, E. and Yavuz, M. (2016), "On the static stability of nonlocal nanobeams using higher-order beam theories", *Adv. Nano Res.*, **4**(1), 51. https://doi.org/10.12989/anr.2016.4.1.051

Eltaher, M.A., Fouda, N., El-midany, T. and Sadoun, A.M. (2018), "Modified porosity model in analysis of functionally graded porous nanobeams", *J. Brazil. Soc. Mech. Sci. Eng.*, **40**, 1-10. https://doi.org/10.1007/s40430-018-1065-0

Eringen, A.C. (1983), "On differential equations of nonlocal elasticity and solutions of screw dislocation and surface waves", *J. Appl. Phys.*, **54**, 4703-4710. https://doi.org/10.1063/1.332803

Eringen, A.C. and Suhubi, E.S. (1964), "Nonlinear theory of simple micro-elastic solids—I", *Int. J. Eng. Sci.*, **2**, 189-203. https://doi.org/https://doi.org/10.1016/0020-7225(64)90004-7

Esmaeilzadeh, M., Esmaeil Golmakani, M., Kadkhodayan, M., Amoozgar, M. and Bodaghi, M. (2021), "Geometrically nonlinear thermo-mechanical analysis of graphene-reinforced moving polymer nanoplates", *Adv. Nano Res.*, **10**(2), 151-163. https://doi.org/10.12989/anr.2021.10.2.151

Faroughi, S., Rahmani, A. and Friswell, M.I. (2020), "On wave propagation in two-dimensional functionally graded porous rotating nano-beams using a general nonlocal higher-order beam model", *Appl. Math. Modell.*, **80**, 169-190. https://doi.org/10.1016/j.apm.2019.11.040

Frýba, L. (1999), *Vibration of Solids and Structures under Moving Loads*, Thomas Telford Publishing. https://doi.org/10.1680/vosasuml.35393

Gayen, D. (2022), "Analysis of temperature, displacement, and stress in shafts made of functionally graded materials with various grading laws", *Adv. Eng. Mater.*, **24**(5), 2101328. https://doi.org/10.1002/adem.202101328

Gayen, D., Tiwari, R. and Chakraborty, D. (2019), "Static and dynamic analyses of cracked functionally graded structural components: A review", *Compos. Part B Eng.*, **173**, 106982. https://doi.org/10.1016/j.compositesb.2019.106982

Gayen, D., Tiwari, R. and Chakraborty, D. (2021), "Thermo-Mechanical Analysis of a Rotor-Bearing System Having a Functionally Graded Shaft with Transverse Breathing Cracks", *In Proceedings of the 6th National Symposium on Rotor*

Dynamics. Springer, Singapore. https://doi.org/10.1007/978-981-15-5701-98

Ghandourah, E.E., Ahmed, H.M., Eltaher, M.A., Attia, M.A. and Abdraboh, A.M. (2021), "Free vibration of porous FG nonlocal modified couple nanobeams via a modified porosity model", *Adv. Nano Res.*, **11**(4), 405-422. https://doi.org/10.12989/anr.2021.11.4.405

Ghandourah, E.E. and Abdraboh, A.M. (2020), "Dynamic analysis of functionally graded nonlocal nanobeam with different porosity models", *Steel Compos. Struct.*, **36**, 293-305. https://doi.org/10.12989/scs.2020.36.3.293

Giannopoulos, G.I., Kakavas, P.A. and Anifantis, N.K. (2008), "Evaluation of the effective mechanical properties of single walled carbon nanotubes using a spring based finite element approach", *Comput. Mater. Sci.*, **41**, 561-569. https://doi.org/https://doi.org/10.1016/j.commatsci.2007.05.016

Huang, X.L. and Shen, H.S. (2004), "Nonlinear vibration and dynamic response of functionally graded plates in thermal environments", *Int. J. Solids Struct.*, **41**, 2403-2427. https://doi.org/10.1016/j.ijsolstr.2003.11.012

Jalaei, M.H. and Arani, A.G. (2018), "Analytical solution for static and dynamic analysis of magnetically affected viscoelastic orthotropic double-layered graphene sheets resting on viscoelastic foundation", *Physica B*, **530**, 222-235. https://doi.org/10.1016/j.physb.2017.11.049

Jalaei, M.H. and Civalek, O (2019), "On dynamic instability of magnetically embedded viscoelastic porous FG nanobeam", *Int. J. Eng. Sci.*, **143**, 14-32. https://doi.org/10.1016/j.ijengsci.2019.06.013

Jalaei, M.H. and Thai, H.T. (2019), "Dynamic stability of viscoelastic porous FG nanoplate under longitudinal magnetic field via a nonlocal strain gradient quasi-3D theory", *Compos. Part B Eng.*, **175**, 107164. https://doi.org/10.1016/j.compositesb.2019.107164

Jankowski, P., Żur, K.K., Kim, J., Lim, C.W. and Reddy, J.N. (2021), "On the piezoelectric effect on stability of symmetric FGM porous nanobeams", *Compos. Struct.*, **267**. https://doi.org/10.1016/j.compstruct.2021.113880

Ke, L.L., Wang, Y.S., Yang, J. and Kitipornchai, S. (2012), "Nonlinear free vibration of size-dependent functionally graded microbeams", *Int. J. Eng. Sci.*, **50**, 256-267. https://doi.org/10.1016/J.IJENGSCI.2010.12.008

Kiani, Y. (2017), "Thermal post-buckling of FG-CNT reinforced composite plates", *Compos. Struct.*, **159**, 299-306. https://doi.org/10.1016/j.compstruct.2016.09.084.

Kim, J., Żur, K.K. and Reddy, J.N. (2019), "Bending, free vibration, and buckling of modified couples stress-based functionally graded porous micro-plates", *Compos. Struct.*, **209**, 879-888. https://doi.org/10.1016/j.compstruct.2018.11.023.

Kong, S., Zhou, S., Nie, Z. and Wang, K. (2008), "The size-dependent natural frequency of Bernoulli-Euler micro-beams", *Int. J. Eng. Sci.*, **46**, 427-437. https://doi.org/10.1016/j.ijengsci.2007.10.002

Kraus, J. (1992), *Electromagnetics*, McGraw-Hill.

Li, L. and Hu, Y. (2015), "Buckling analysis of size-dependent nonlinear beams based on a nonlocal strain gradient theory", *Int. J. Eng. Sci.*, **97**, 84-94. https://doi.org/10.1016/j.ijengsci.2015.08.013

Li, L. and Hu, Y. (2016), "Nonlinear bending and free vibration analyses of nonlocal strain gradient beams made of functionally graded material", *Int. J. Eng. Sci.*, **107**. https://doi.org/10.1016/j.ijengsci.2016.07.011

Li, L., Pratihar, D.K., Chakrabarty, S. and Mishra, P.C. (2020), *Advances in Materials and Manufacturing Engineering*, **119**(125), Springer. https://doi.org/10.1007/978-981-15-1307-7

Lim, C.W., Zhang, G. and Reddy, J.N. (2015), "A higher-order nonlocal elasticity and strain gradient theory and its applications in wave propagation", *J. Mech. Phys. Solids*, **78**, 298-313. https://doi.org/10.1016/j.jmps.2015.02.001

Liu, H., Liu, H. and Yang, J. (2018), "Vibration of FG magneto-electro-viscoelastic porous nanobeams on visco-Pasternak foundation", *Compos. Part B Eng.*, **155**, 244-256. https://doi.org/10.1016/j.compositesb.2018.08.042

Merzouki, T., Ahmed, H.M.S., Bessaim, A., Haboussi, M., Dimitri, R. and Tornabene, F. (2021), "Bending analysis of functionally graded porous nanocomposite beams based on a non-local strain gradient theory", *Math. Mech. Solids*, **27**(1), 66-92. https://doi.org/10.1177/10812865211011759

Najafi, F., Shojaeefard, M.H. and Googarchin, H.S. (2017), "Nonlinear dynamic response of FGM beams with Winkler-Pasternak foundation subject to noncentral low velocity impact in thermal field", *Compos. Struct.*, **167**, 132-143. https://doi.org/https://doi.org/10.1016/j.compstruct.2017.01.063.

Nikrad, S.F., Kanellopoulos, A., Bodaghi, M., Chen, Z.T. and Pourasghar, A. (2021), "Large deformation behavior of functionally graded porous curved beams in thermal environment", *Arch. Appl. Mech.*, **91**, 2255-2278. https://doi.org/10.1007/s00419-021-01882-9

Oguamanam, D.C.D., Hansen, J.S. and Heppler, G.R. (1998), "Dynamic response of an overhead crane system", *J. Sound Vib.*, **213**, 889-906. https://doi.org/https://doi.org/10.1006/jsvi.1998.1564

Pandey, S. and Pradyumna, S. (2015), "Free vibration of functionally graded sandwich plates in thermal environment using a layerwise theory", *Eur. J. Mech. A Solids*, **51**, 55-66. https://doi.org/10.1016/j.euromechsol.2014.12.001

Penna, R., Feo, L. and Lovisi, G. (2021a), "Hygro-thermal bending behavior of porous FG nano-beams via local/nonlocal strain and stress gradient theories of elasticity", *Compos. Struct.*, **263**, 113627. https://doi.org/10.1016/j.compstruct.2021.113627

Penna, R., Feo, L., Lovisi, G. and Fabbrocino, F. (2021b), "Hygro-thermal vibration of porous fg nano-beams based on local/ nonlocal stress gradient theory of elasticity", *Nanomaterials*, **11**, 1-16. https://doi.org/10.3390/nano11040910

Rahmani, A., Faroughi, S. and Friswell, M.I. (2020a), "The vibration of two-dimensional imperfect functionally graded (2D-FG) porous rotating nanobeams based on general nonlocal theory", *Mech. Syst. Signal Pr.*, **144**, 106854. https://doi.org/10.1016/j.ymssp.2020.106854

Rahmani, F., Kamgar, R. and Rahgozar, R. (2020b), "Finite element analysis of functionally graded beams using different beam theories", *Civil Eng. J.*, **6**, 2086-2102. https://doi.org/10.28991/cej-2020-03091604

Reddy, J.N. (1984), "A simple higher-order theory for laminated composite plates", *J. Appl. Mech.*, **51**, 745-752. https://doi.org/10.1115/1.3167719

Reddy, J.N. (2007), "Nonlocal theories for bending, buckling and vibration of beams", *Int. J. Eng. Sci.*, **45**, 288-307. https://doi.org/10.1016/j.ijengsci.2007.04.004

Reddy, J.N. and Chin, C.D. (1998), "Thermomechanical analysis of functionally graded cylinders and plates", *J. Therm. Stress.*, **21**, 593-626. https://doi.org/10.1080/01495739808956165

Salari, E., Sadough Vanini, S.A., Ashoori, A.R. and Akbarzadeh, A.H. (2020), "Nonlinear thermal behavior of shear deformable FG porous nanobeams with geometrical imperfection: Snap-through and postbuckling analysis", *Int. J. Mech. Sci.*, **178**, 105615. https://doi.org/10.1016/j.ijmecsci.2020.105615

Saleh, B., Jiang, J., Fathi, R., Al-hababi, T., Xu, Q., Wang, L., Song, D. and Ma, A. (2020), "30 Years of functionally graded materials: An overview of manufacturing methods, applications and future challenges", *Compos. Part B Eng.*, **201**, 108376. https://doi.org/10.1016/j.compositesb.2020.108376

Shafiei, N. and Kazemi, M. (2017), "Nonlinear buckling of

functionally graded nano-/micro-scaled porous beams", *Compos. Struct.*, **178**, 483-492. https://doi.org/10.1016/j.compstruct.2017.07.045

She, G.L., Ren, Y.R. and Yan, K.M. (2019), "On snap-buckling of porous FG curved nanobeams", *Acta Astronaut.*, **161**, 475-484. https://doi.org/10.1016/j.actaastro.2019.04.010

Sobhy, M. (2015), "Hygrothermal deformation of orthotropic nanoplates based on the state-space concept", *Compos. Part B Eng.*, **79**, 224-235. https://doi.org/10.1016/j.compositesb.2015.04.042

Srinivas, S. and Rao, A.K. (1970), "Bending, vibration and buckling of simply supported thick orthotropic rectangular plates and laminates", *Int. J. Solid Struct.*, **6**, 1463-1481. https://doi.org/https://doi.org/10.1016/0020-7683(70)90076-4

Talebizadehsardari, P., Salehipour, H., Shahgholian-Ghahfarokhi, D., Shahsavar, A. and Karimi, M. (2020), "Free vibration analysis of the macro-micro-nano plates and shells made of a material with functionally graded porosity: A closed-form solution", *Mech. Based Des. Struct. Mach.*, 1-27. https://doi.org/10.1080/15397734.2020.1744002

Touloukian, Y.S. (1967), *Thermophysical Properties of High Temperature Solid Materials*, Macmillan, New York, U.S.A.

Wang, Y., Xie, K. and Fu, T. (2018), "Vibration analysis of functionally graded porous shear deformable tubes excited by moving distributed loads", *Acta Astronaut.*, **151**, 603-613. https://doi.org/https://doi.org/10.1016/j.actaastro.2018.06.003

Wu, D., Liu, A., Huang, Y., Huang, Y., Pi, Y. and Gao, W. (2018), "Dynamic analysis of functionally graded porous structures through finite element analysis", *Eng. Struct.*, **165**, 287-301. https://doi.org/10.1016/j.engstruct.2018.03.023

Xu, X., Karami, B. and Shahsavari, D. (2021), "Time-dependent behavior of porous curved nanobeam", *Int. J. Eng. Sci.*, **160**. https://doi.org/10.1016/j.ijengsci.2021.103455

Yaylı, M.Ö. (2015), "Buckling analysis of a rotationally restrained single walled carbon nanotube", *Acta Phys. Pol. A*, **127**(3), 678-683. https/doi.org/10.12693/APhysPolA.127.678

Yayli, M.Ö. (2016), "Buckling analysis of a microbeam embedded in an elastic medium with deformable boundary conditions", *Micro Nano Lett.*, **11**(11), 741-745. https://doi.org/10.1049/mnl.2016.0257

Yayli, M.Ö. (2018a), "Free longitudinal vibration of a nanorod with elastic spring boundary conditions made of functionally graded material", *Micro Nano Lett.*, **13**(7), 1031-1035. https://doi.org/10.1049/mnl.2018.0181

Yayli, M.Ö. (2018b), "Free vibration analysis of a single-walled carbon nanotube embedded in an elastic matrix under rotational restraints", *Micro Nano Lett.*, **13**(2), 202-206. https://doi.org/10.1049/mnl.2017.0463

Yayli, M.Ö. (2018c), "Torsional vibration analysis of nanorods with elastic torsional restraints using non-local elasticity theory", *Micro Nano Lett.*, **13**(5), 595-599. https://doi.org/10.1049/mnl.2017.0751

Yayli, M.Ö. (2019a), "Effects of rotational restraints on the thermal buckling of carbon nanotube", *Micro Nano Lett.*, **14**(2), 158-162. https://doi.org/10.1049/mnl.2018.5428

Yayli, M.Ö. (2019b), "Free vibration analysis of a rotationally restrained (FG) nanotube", *Microsyst. Technol.*, **25**(10), 3723-3734. https://doi.org/10.1007/s00542-019-04307-4

Yayli, M.Ö. (2020), "Axial vibration analysis of a Rayleigh nanorod with deformable boundaries", *Microsyst. Technol.*, **26**(8), 2661-2671. https://doi.org/10.1007/s00542-020-04808-7